Neuron, Vol. 41, 677–682, March 4, 2004, Copyright ©2004 by Cell Press

Polyglutamine Diminishes VEGF: Passage to Motor Neuron Death?

Altered gene transcription has been implicated in the pathogenesis of polyglutamine-dependent neurodegeneration. In this issue of *Neuron*, Sopher et al. demonstrate that androgen receptors containing expanded polyglutamine cause decreased expression of vascular endothelial growth factor (VEGF) by interfering with cAMP response element binding protein binding protein (CBP), thereby contributing to the motor neuron degeneration in spinal and bulbar muscular atrophy.

Expansion of a triplet nucleotide repeat is the molecular basis for a variety of hereditary neuromuscular diseases. At least nine neurodegenerative diseases result from a tedious trinucleotide CAG repeat, which encodes a polyglutamine tract (reviewed in Zoghbi and Orr, 2000). These disorders, called polyglutamine diseases, include spinal and bulbar muscular atrophy (SBMA), Huntington's disease (HD), spinocerebellar ataxias (SCA1, 2, 3, 6, 7, and 17), and dentatorubral pallidoluysian atrophy (DRPLA). Several shared clinical and histopathological features seen in polyglutamine diseases imply a common pathogenesis. The patients suffer from slow progressive neuromuscular symptoms with the onset in adulthood. Although the causative genes are distinct, selected subsets of neurons in the central nervous system undergo degeneration in each disease. Histopathological hallmarks are the loss of neurons in the affected area and the existence of characteristic intranuclear inclusions in the residual neuronal cells. These inclusions contain aggregates of the causative protein together with fundamental cellular components, providing a clue to the mechanisms causing neurodegeneration. Although the precise role of these inclusions remains open to debate, a large body of evidence suggests that the nuclear localization of aberrant polyglutamine protein is an essential step in the pathogenesis.

The perturbation of gene transcription is likely to be among the most substantial nuclear events in the pathophysiology of polyglutamine diseases. This hypothesis emerged from the observation that cAMP response element binding protein binding protein (CBP), a transcriptional coactivator, is sequestrated into the polyglutamine inclusion (Nucifora et al., 2001). Furthermore, the acetyltransferase activity of CBP is directly inhibited by the interaction with aberrant polyglutamine protein (Steffan et al., 2001). In agreement with these findings, alteration of a wide range of gene expression has been detected in mouse models of polyglutamine diseases (Sugars and Rubinsztein, 2003). It is of therapeutic significance that polyglutamine-mediated neurodegeneration in a *Drosophila* model of HD is alleviated by histone deacetylase inhibitors, which restore histone acetylation and upregulate gene transcriptions (Steffan et al., 2001). Although decreased transcription appears to be a plausible explanation for the pathogenesis, little direct link between CBP dysfunction and neurodegeneration has been clarified in vivo. In addition, it remains unclear which gene is responsible for neuronal cell death in each polyglutamine disease.

Spinal and bulbar muscular atrophy (SBMA), or Kennedy's disease, which is caused by an expanded CAG repeat in the androgen receptor (AR) gene, was the first disease to be identified as a polyglutamine disease (La Spada et al., 1991). SBMA is an adult-onset lower motor neuron disease characterized by proximal muscle atrophy, weakness, fasciculations, and bulbar involvement. In the central nervous system, the brainstem and the anterior horn are selectively involved. Besides motor neuron degeneration, patients present with several systemic complications: gynecomastia, hyperlipidemia, and glucose intolerance. Since the loss of AR function does not result in neuromuscular phenotypes, the extended polyglutamine tract itself appears to render the causative protein toxic, as documented in other polyglutamine diseases. The disruption of CBP-mediated transcription has also been implicated in the pathogenesis of this disease (McCampbell et al., 2001). Despite a common molecular basis, SBMA is distinct from other polyglutamine diseases in that males are exclusively affected. A transgenic mouse model of SBMA revealed that ligand-dependent nuclear translocation of the pathogenic AR protein accounts for the gender-related pathogenesis, leading to the development of a potential hormonal therapy for this disorder (Katsuno et al., 2002). In this issue of *Neuron*, Sopher et al. (2004) report a new transgenic mouse model carrying human AR yeast artificial chromosome (YAC) with a prolonged CAG repeat. Their study reconfirmed the importance of nuclear accumulation of aberrant AR and ligand-dependent pathophysiology in SBMA. Since the expression of the transgene is controlled by its own promoter, the mRNA level of the mutant AR in this model is less than that in previous mouse models using potent exogenous promoters. This would account for the pathological distribution reminiscent of SBMA and the slow progression of motor disability. Among the conspicuous achievements in this study is the finding that the transgenic mice recapitulate the loss of lower motor neurons in SBMA. Whereas histopathological studies of autopsy cases with polyglutamine diseases show a tangible loss of neurons in lesions, a majority of transgenic mouse models demonstrate neuromuscular disability without detectable cell death (Zoghbi and Orr, 2000). This could be explained by the short life span and excessive expression of the causative polyglutamine protein in these mouse models. Symptomatic phenotypes with normal cell populations may indicate that the pathophysiology of polyglutamine disease rises from the dysfunction of neurons. This hypothesis in turn indicates the reversibility of the pathogenesis at the early stage of the diseases. In support of this view, the interruption of mutant gene

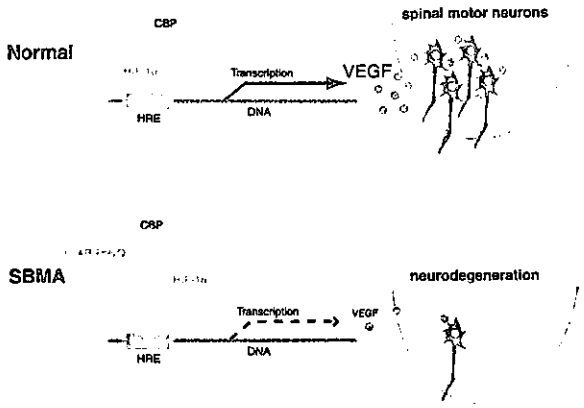

Figure 1. Possible Mechanism of VEGF-Related Motor Neuron Degeneration in SBMA

Hypoxia-inducible factor 1α (HIF-1α) binds to hypoxia-response element (HRE) in the promoter of vascular endothelial growth factor (VEGF), upregulating its transcription. This transactivating activity of HIF-1α is facilitated through interaction with cAMP response element binding protein binding protein (CBP). In spinal and bulbar muscular atrophy (SBMA), the pathogenic androgen receptor (AR) containing expanded polyglutamine (polyQ) interacts with CBP, resulting in decreased level of VEGF. These processes appear to contribute to motor neuron degeneration in SBMA.

expression reversed the symptoms and histopathological features in a conditional mouse model of HD using a tet-regulation system (Yamamoto et al., 2000). Although this observation justifies medical intervention to mildly affected or presymptomatic patients, elucidating the precise mechanism giving rise to neuronal cell death is also essential for the development of therapies for polyglutamine diseases. The study of Sopher et al. appears to offer a striking insight into the pathophysiology of polyglutamine-induced motor neuron death, in their revelation that the interaction between pathogenic AR and CBP results in a reduced expression of vascular endothelial growth factor (VEGF), which appears to contribute to the neurodegeneration in SBMA.

VEGF, first discovered as a factor enhancing vascular permeability, plays a crucial role in physiological and pathological angiogenesis. Diverse biological effects of VEGF are facilitated by its receptor, VEGF-2, also termed kinase insert domain receptor (KDR). The gene expression of VEGF is drastically upregulated upon hypoxia in order to form new blood vessels. Hypoxia-inducible factors, HIF-1α and HIF-2α, mediate this cellular protective response through binding to hypoxia-response element (HRE) in the promoter of VEGF. The transactivating activity of HIF-1α is facilitated through interaction with transcriptional coactivators such as CBP (Figure 1). The depletion of a single allele of VEGF results in embryonic lethality, whereas lack of the HRE sequence in the VEGF promoter leads to slowly progressive motor neuron degeneration (Oosthuyse et al., 2001). Knockin mice harboring a *VEGF* gene in which HRE is deleted demonstrate a late-onset motor neuron disease resembling SBMA and amyotrophic lateral sclerosis (ALS), suggesting a pivotal role for VEGF in neurodegeneration. The low expression level of VEGF in these mice results in loss of spinal motor neurons, axonal degeneration in the peripheral nerve, and neurogenic muscular atrophy, all of which are pathological features of human motor neuron diseases. Moreover, the targeted disruption of HRE results in the marked exacerbation of motor neuron degeneration in transgenic mice carrying mutant superoxide dismutase 1 (SOD 1), the most frequent cause of familial ALS (Lambrechts et al., 2003). The deleterious effects of HRE deletion on motor neurons could be due to the suppression of favorable effects of VEGF: enhancement of blood supply and direct neuroprotection. Given that intraperitoneal administration of VEGF ameliorates ischemia-induced degeneration of spinal motor neurons in the aberrant VEGF knockin mice (Lambrechts et al., 2003), blood circulation insufficiency may cause neuromuscular phenotypes. Since VEGF protects cultured normal motor neurons from apoptotic stimuli, loss of these neurotrophic effects could also contribute to the pathogenesis of motor neuron degeneration due to HRE deletion.

The study of Sopher et al. shows that the reduction in the expression level of VEGF precedes the onset of neurogenic muscular atrophy, suggesting that the transcriptional alteration is a trigger, rather than a consequence, of neurodegeneration. The implication of VEGF in SBMA is also backed by the observation that an exogenous VEGF administration alleviates cytotoxicity induced by pathogenic AR with expanded polyglutamine in their cell model. In addition, CBP cotransfection augments VEGF level in the same cultured motor neurons, implying that the transactivating ability of CBP is suppressed by an aberrant protein-protein interaction with AR. This work sheds light on VEGF as a key player in the pathogenesis of polyglutamine-induced motor neuron degeneration, providing another therapeutic target for SBMA. The retrograde delivery of neurotrophic factors ameliorates neurodegeneration in mouse models of motor neuron diseases to some extent (Kaspar et al., 2003). It should be of value to investigate whether VEGF administration improves the polyglutamine-dependent pathogenesis in the SMBA mouse model of Sopher et al. Alternatively, the repressed transcription of VEGF in SBMA mice suggests that chronic hypoxia aggravates motor neuron degeneration, although its clinical implications have yet to be elucidated. Chronic ischemia, aggravated by lowered level of VEGF, appears to induce oxidative stress, which has been suggested to exacerbate neurodegenerative processes. It thus seems possible that polyglutamine-induced pathophysiology could be ameliorated by antioxidative therapy, which should be tested elsewhere.

A great deal of effort has been made to clarify the exact mechanism causing neuronal dysfunction and the process leading to cell death in polyglutamine diseases. Multiple pathophysiological steps may plunge neurons from dysfunction to death in the presence of an expanded polyglutamine tract. The transcriptional dysregulation of VEGF is likely to play an important role in polyglutamine-induced motor neuron death, since the HRE-deleted mice also showed loss of spinal motor neurons (Oosthuyse et al., 2001). However, whether this hypothesis accounts for the whole pathogenesis of SBMA remains to be resolved. Given that multiple mechanisms are involved in neurodegeneration, we need to clarify which genes, regulated by CBP or other factors,

are responsible for the pathogenesis of polyglutamine diseases. Such clarification would expand therapeutic options for these devastating disorders.

Masahisa Katsuno and Gen Sobue
Department of Neurology
Nagoya University Graduate School of Medicine
Nagoya 466-8550
Japan

Selected Reading

Katsuno, M., Adachi, H., Kume, A., Li, M., Nakagomi, Y., Niwa, H., Sang, C., Kobayashi, Y., Doyu, M., and Sobue, G. (2002). Neuron *35*, 843–854.

Kaspar, B.K., Llado, J., Sherkat, N., Rothstein, J.D., and Gage, F.H. (2003). Science *301*, 839–842.

Lambrechts, D., Storkebaum, E., Morimoto, M., Del-Favero, J., Desmet, F., Marklund, S.L., Wyns, S., Thijs, V., Andersson, J., van Marion, I., et al. (2003). Nat. Genet. *34*, 383–394.

La Spada, A.R., Wilson, E.M., Lubahn, D.B., Harding, A.E., and Fischbeck, K.H. (1991). Nature *352*, 77–79.

McCampbell, A., Taye, A.A., Whitty, L., Penney, E., Steffan, J.S., and Fischbeck, K.H. (2001). Proc. Natl. Acad. Sci. USA *98*, 15179–15184.

Nucifora, F.C., Jr., Sasaki, M., Peters, M.F., Huang, H., Cooper, J.K., Yamada, M., Takahashi, H., Tsuji, S., Troncoso, J., Dawson, V.L., et al. (2001). Science *291*, 2423–2428.

Oosthuyse, B., Moons, L., Storkebaum, E., Beck, H., Nuyens, D., Brusselmans, K., Van Dorpe, J., Hellings, P., Gorselink, M., Heymans, S., et al. (2001). Nat. Genet. *28*, 131–138.

Sopher, B.L., Thomas, P.S., Jr., LaFevre-Bernt, M.A., Holm, I.E., Wilke, S.A., Ware, C.B., Jin, L.-W., Libby, R.T., Ellerby, L.M., and La Spada, A.R. (2004). Neuron *41*, this issue, 687–699.

Steffan, J.S., Bodai, L., Pallos, J., Poelman, M., McCampbell, A., Apostol, B.L., Kazantsev, A., Schmidt, E., Zhu, Y.Z., Greenwald, M., et al. (2001). Nature *413*, 739–743.

Sugars, K.L., and Rubinsztein, D.C. (2003). Trends Genet. *19*, 233–238.

Yamamoto, A., Lucas, J.J., and Hen, R. (2000). Cell *101*, 57–66.

Zoghbi, H.Y., and Orr, H.T. (2000). Annu. Rev. Neurosci. *23*, 217–247.

Migraine Aura: A Knockin Mouse with a *Knockout* Message

Migraine aura is a sometimes disabling disorder of the brain that involves significant neurological symptoms in about 30% of patients. In this issue of *Neuron*, van den Maagdenberg et al. characterize a mouse with a knockin mutation known to cause familial hemiplegic migraine and provide evidence that a lowered threshold to the triggering of CSD may account for the devastating phenotype of familial hemiplegic migraine.

A good basic neuroscience paper can illustrate a fundamental principle, exploit new methods to open avenues for study, or even point the general direction to the horizon where novel therapies will be found. This issue of the *Neuron* has a contribution that does each of these (van den Maagdenberg et al., 2004). Beginning to model aspects of the most common of the severely disabling forms of primary headache delivers the *knockout* message that common neurobiological problems will yield secrets to basic neuroscience for the ultimate good of patients.

Migraine aura consists of the neurological symptoms, flashing jagged lights, pins and needles, or even weakness, that are so well recognized as preceding the attack proper in about 30% of patients. Familial hemiplegic migraine is a very rare form of migraine with prolonged aura in which an important manifestation is one-sided weakness. So far, from a clinical viewpoint, it has been difficult to dissect its various forms. Mutations in the *CACNA1A* gene that encodes the pore-forming subunit of the P/Q voltage-gated calcium channel ($Ca_V2.1$) cause about 50% of this disorder (Ophoff et al., 1996). In addition, perhaps 30% of patients might be accounted for by mutations in *ATP1A2* gene that encodes the Na^+/K^+ pump α_2 subunit (De Fusco et al., 2003). Both of these changes could lead to increases in intracellular Ca^{2+}, but this has raised the essential "so what" problem: how does this elegant biology enlighten the clinical question, why would this result in episodic, often profound weakness?

Cortical spreading depression is a wave of excitation followed by inhibition that traverses the cortex at a rate of about 3–6 mm/min Pioneering work using human brain blood flow measurements during migraine aura showed that the flow changes associated with aura also moved at this curious slow rate across the brain. Brain imaging (Hadjikhani et al., 2001) has carefully built a case that migraine aura is the human version of the cortical spreading depression measured by electrophysiological methods in experimental animals (Lauritzen, 1994). Studies of migraine aura in humans and cortical spreading depression in experimental animals have led to some very important questions: how is aura triggered in humans, what role might the genetic mutations described above in familial hemiplegic migraine play, and last, what is the role of aura in migraine—is it the pain trigger?

In this issue of *Neuron*, van den Maagdenberg and colleagues report a *Cacna1a* knockin mouse with increased susceptibility to cortical spreading depression. Using the R192Q mutation, which is clearly pathogenic in humans (Ophoff et al., 1996), they very elegantly characterize with electrophysiological methods a gain-of-function in cerebellar granule cells in culture from homozygous mice. At the neuromuscular junction, endplate potentials, used as a measure of acetylcholine-evoked postsynaptic depolarizations, were increased by 240% under conditions of low Ca^{2+} concentration, representing enhanced activation in mutant mice compared to wild-type mice. Using DC potential recordings at the cortex, the authors also noted a lowered threshold for the induction and a remarkable 150% increase in the rate of propagation of cortical spreading depression. Previous work using electrophysiological techniques had shown a gain-of-function at the channel level but a loss-of-function at the whole-cell level in transfected cells that van den Maagdenberg and colleagues attribute to overexpression. A general principle illustrated by the new work is the absolute necessity for whole-animal studies to dissect the effects of mutations and understand the integrated physiology of a disease. Rely-

Journal of Neurochemistry, 2004, **89**, 64–72 doi:10.1046/j.1471-4159.2003.02289.x

Dorfin prevents cell death by reducing mitochondrial localizing mutant superoxide dismutase 1 in a neuronal cell model of familial amyotrophic lateral sclerosis

Hideyuki Takeuchi, Jun-ichi Niwa, Nozomi Hishikawa, Shinsuke Ishigaki, Fumiaki Tanaka, Manabu Doyu and Gen Sobue

Department of Neurology, Nagoya University Graduate School of Medicine, 65 Tsurumai-cho, Showa-ku, Nagoya 466-8550, Japan

Abstract

Dorfin is a RING-finger type ubiquitin ligase for mutant superoxide dismutase 1 (SOD1) that enhances its degradation. Mutant SOD1s cause familial amyotrophic lateral sclerosis (FALS) through the gain of unelucidated toxic properties. We previously showed that the accumulation of mutant SOD1 in the mitochondria triggered the release of cytochrome *c*, followed by the activation of the caspase cascade and induction of neuronal cell death. In the present study, therefore, we investigated whether Dorfin can modulate the level of mutant SOD1 in the mitochondria and subsequent caspase activation. We showed that Dorfin significantly reduced the amount of mutant SOD1 in the mitochondria, the release of cytochrome *c* and the activation of the following caspase cascade, thereby preventing eventual neuronal cell death in a neuronal cell model of FALS. These results suggest that reducing the accumulation of mutant SOD1 in the mitochondria may be a new therapeutic strategy for mutant SOD1-associated FALS, and that Dorfin may play a significant role in this.

Keywords: amyotrophic lateral sclerosis, Dorfin, mitochondria, neuronal cell death, superoxide dismutase 1, ubiquitin ligase.

J. Neurochem. (2004) **89**, 64–72.

Amyotrophic lateral sclerosis (ALS) is a fatal neurodegenerative disease caused by selective death of motor neurons. Approximately 10% of ALS cases are familial (FALS). Missense mutations in the gene coding superoxide dismutase 1 (SOD1) are responsible for approximately 20% of FALS cases (Rosen *et al.* 1993; Hirano 1996) through the gain of unelucidated toxic properties (Yim *et al.* 1996).

Many reports have documented that the mitochondria are involved in the pathogenic process in mutant SOD1-associated FALS. Mitochondrial degeneration, including swelling, dilatation and vacuolization, is an early characteristic pathological feature of FALS and FALS transgenic (Tg) mice models with SOD1 mutations (Dal Canto and Gurney 1994; Wong *et al.* 1995; Hirano 1996; Kong and Xu 1998; Jaarsma *et al.* 2000; Higgins *et al.* 2003). Recently, it was demonstrated that SOD1, considered to be a cytosolic enzyme, exists in the mitochondria (Sturtz *et al.* 2001; Okado-Matsumoto and Fridovich 2001; Higgins *et al.* 2002), and that the mitochondrial vacuoles in mutant SOD1 Tg mice were lined with mutant SOD1 (Jaarsma *et al.* 2001; Higgins *et al.* 2003). Many studies have suggested that the programmed cell death (PCD) pathway contributes to motor neuron death in FALS (Durham *et al.* 1997; Martin 1999; Li *et al.* 2000; Pasinelli *et al.* 2000; Guégan *et al.* 2001; Kriz *et al.* 2002; Raoul *et al.* 2002; Zhu *et al.* 2002). Moreover, we previously reported that accumulation of mutant SOD1 in the mitochondria triggered the release of mitochondrial cytochrome *c*, which subsequently activated the caspase cascade and induced neuronal cell death (Takeuchi *et al.* 2002a). Taken together, these results suggest that the accumulation of mutant SOD1 in the mitochondria is critical in the pathogenesis of mutant SOD1-associated FALS.

Received September 23, 2003; revised manuscript received November 17, 2003; accepted November 24, 2003.

Address correspondence and reprint requests to Gen Sobue, Department of Neurology, Nagoya University Graduate School of Medicine, 65 Tsurumai-cho, Showa-ku, Nagoya 466-8550, Japan.
E-mail: sobueg@med.nagoya-u.ac.jp

Abbreviations used: ALS, amyotrophic lateral sclerosis; COX, cytochrome *c* oxidase; DMEM, Dulbecco's modified Eagle's medium; E3, ubiquitin ligase; EGFP, enhanced green fluorescent protein; FALS, familial amyotrophic lateral sclerosis; MTS, 3-(4,5-dimethyl-thiazol-2yl)-5-(3-carboxymethoxyphenyl)-2-(4-sulfophenyl)-2H-tetrazolium; PCD, programmed cell death; PI, propidium iodide; SOD1, superoxide dismutase 1; Tg, transgenic.

Dorfin is the product of a gene that we cloned from the anterior horn tissue of the human spinal cord (Niwa *et al.* 2001); it contains a RING-finger/IBR motif (Niwa *et al.* 2001) at its N-terminus. It was reported that a distinct subclass of RING-finger/in-between RING-fingers (IBR) motif-containing proteins represents a new ubiquitin ligase (E3) family that interacts specifically with distinct ubiquitin-conjugating enzymes (Moynihan *et al.* 1999; Ardley *et al.* 2001). Dorfin is a juxtanuclearly located E3 that ubiquitylates various SOD1 mutants derived from patients with FALS, and enhances the degradation of mutant SOD1 (Niwa *et al.* 2002). Whether Dorfin can modulate the protein level of mutant SOD1 in the mitochondria, and the subsequent activation of the mitochondrial caspase cascade, is an important and interesting question.

Here we show that Dorfin significantly reduced the amount of mutant SOD1 in mitochondria, the release of cytochrome *c* from mitochondria into the cytosol and the subsequent activation of the caspase cascade, thereby preventing the eventual neuronal cell death in a neuronal cell model of FALS. These results suggest that reducing mutant SOD1 in the mitochondria may be a useful strategy for the treatment of mutant SOD1-associated FALS, and that Dorfin might play a significant role in this.

Materials and methods

Plasmids

Non-organelle-oriented plasmids expressing the enhanced green fluorescent protein (EGFP)-tagged human SOD1 (wild type, mutant G93A, and G85R) were described previously (Takeuchi *et al.* 2002a,b). These vectors express SOD1-EGFP fusion proteins ubiquitously in each organelle (Takeuchi *et al.* 2002a). They were designated Cyto-WT, Cyto-G93A and Cyto-G85R respectively. Mitochondria-oriented plasmids expressing EGFP-tagged human SOD1 (wil dtype, mutant G93A and G85R) with mitochondrial localizing signals were generated as described previously (Takeuchi *et al.* 2002a). These vectors express SOD1-EGFP fusion proteins mainly in the mitochondria (Takeuchi *et al.* 2002a). They were designated Mito-WT, Mito-G93A and Mito-G85R respectively. The plasmid pcDNA3.1/HisMax-Dorfin, which expresses Xpress-tagged Dorfin, was also described previously (Niwa *et al.* 2001). As a control, we used pCMV-β vector expressing LacZ (Clontech, Palo Alto, CA, USA). All constructs used here were confirmed by DNA sequence analysis.

Cell culture

Mouse neuroblastoma cell line Neuro2a cells were maintained in Dulbecco's modified Eagle's medium (DMEM) (Invitrogen Corp., Carlsbad, CA, USA) supplemented with 10% fetal calf serum (Invitrogen Corp.) as described previously (Takeuchi *et al.* 2002b). They were cultured on Laboratory-Tec II four-well chamber slides (Nalge Nunc International, Rochester, NY, USA) coated with poly-L-lysine (Sigma, St Louis, MO, USA). Transient expression of SOD1 plasmids (0.1 μg of DNA/well) and pcDNA3.1/His Max-Dorfin or pCMV-β (0.3 μg of DNA/well) in Neuro2a cells (2×10^4 cells/well) was accomplished with LipofectAMINE PLUS reagent (Invitrogen Corp.). After incubation for 3 h with transfection reagents, transfected cells were cultured in differentiation medium (DMEM supplemented with 1% fetal calf serum and 20 μM retinoic acid). To detect Xpress-Dorfin fusion protein, 0.5 μM proteasome inhibitor MG132 (Sigma) was added 16 h before collection, as described previously (Niwa *et al.* 2001).

Cell fractionation

At each time point (0, 24 and 48 h) after transfection, cells were collected and gently homogenized with a Dounce homogenizer in cold buffer [250 mM sucrose, 10 mM Tris-HCl pH 7.5, 5 mM $MgCl_2$, 2 mM EDTA and protease inhibitor cocktail (Complete Mini EDTA-free; Roche Diagnostics, Basel, Switzerland)]. Cell fractionation was performed as described previously (Takeuchi *et al.* 2002a). To verify the fractionation, each fraction was subjected to western blotting for cytochrome *c* oxidase (COX) as a mitochondrial marker using anti-COX subunit IV mouse monoclonal antibody (1 : 1000; Molecular Probes, Eugene, OR, USA), and β-actin as a cytosolic marker using anti-β-actin mouse monoclonal antibody (1 : 5000; Sigma).

Western blot analysis

The protein concentration was determined with a DC protein assay kit (Bio-Rad Laboratories, Hercules, CA, USA) and western blotting was done as described previously (Takeuchi *et al.* 2002b). To evaluate the level of mitochondrially localized SOD1-EGFP fusion proteins, 20 μg protein from the mitochondrial fraction was loaded. For analyzing the release of cytochrome *c* from the mitochondria into the cytosol, 20 μg protein from the mitochondrial fraction or the cytosolic fraction was loaded.

To assess the levels of SOD1-EGFP fusion proteins, Xpress-Dorfin fusion proteins and the activation of caspase-9 and caspase-3, cells were collected at each time point (0, 24 and 48 h) after transfection, and lysed in TNES buffer (50 mM Tris-HCl pH 7.5, 150 mM NaCl, 1% NP-40, 2 mM EDTA, 0.1% sodium dodecyl sulfate and protease inhibitor cocktail) as described previously (Takeuchi *et al.* 2002a). For the analysis, 20 μg protein from the total lysate was loaded.

The primary antibodies used were as follows: anti-SOD1 rabbit polyclonal antibody (1 : 10 000; StressGen Biotechnologies, Victoria, BC, Canada), anti-Xpress mouse monoclonal antibody (1 : 5000; Invitrogen Corp.), anti-caspase-3 rabbit polyclonal antibody and anti-caspase-9 rabbit polyclonal antibody (1 : 1000; Cell Signaling, Beverly, MA, USA) and anti-cytochrome *c* mouse monoclonal antibody (1 : 1000; Pharmingen, San Diego, CA, USA). After overnight incubation with primary antibodies at 4°C, each blot was probed with horseradish peroxidase-conjugated anti-rabbit IgG and anti-mouse IgG (1 : 5000; Amersham Biosciences, Piscataway, NJ, USA). Blots were then visualized with ECL Plus western blotting detection reagents (Amersham Biosciences). The signal intensity was quantified by densitometry using NIH Image 1.63 software.

Immunocytochemistry

At each time point (0, 24 and 48 h) after transfection, cells were fixed with 4% paraformaldehyde for 30 min on ice and then

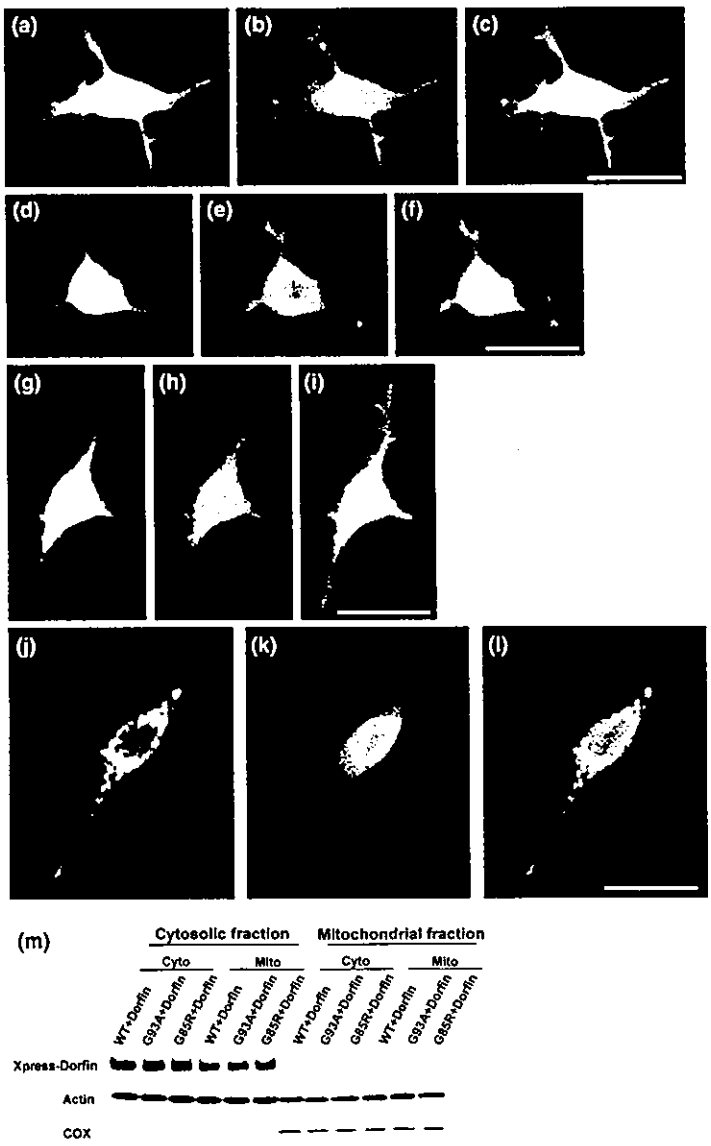

Fig. 1 Subcellular localization of SOD1-EGFP and Xpress-Dorfin in Neuro2a cells. (a–l) Confocal laser scanning microscopic images at 48 h after transfection. (m) Fractionation analysis of Xpress-Dorfin fusion protein. (a–c) Cyto-WT + Xpress-Dorfin, (d–f) Cyto-G93A + Xpress-Dorfin, (g–l) Cyto-G85R + Xpress-Dorfin; (j–l) Mito-G93A + Xpress-Dorfin. SOD1-EGFP fusion proteins (green; a, d and g) and Xpress-Dorfin fusion proteins (red; b, e and h) were observed ubiquitously in the cells with Cyto-SOD1 containing no organelle-oriented signals. SOD1-EGFP fusion proteins and Xpress-Dorfin fusion proteins were co-localized (yellow; c, f and i). In contrast, in the cells with Mito-SOD1, SOD1-EGFP fusion proteins were observed in the mitochondria (green; j) and Xpress-Dorfin fusion proteins (red; k) were observed mainly in the cytoplasm. They were not co-localized in the cells with Mito-SOD1 (l). Cells were counterstained with TO-PRO-3 (blue). Scale bars, 10 μm. Western blots also revealed that Xpress-Dorfin fusion proteins were absent in the mitochondrial fraction (m).

permeabilized with 0.05% Triton X-100 at room temperature for 10 min. They were stained with the anti-Xpress mouse monoclonal antibody (1 : 5000; Invitrogen Corp.) at 4°C overnight. They were subsequently stained with Alexa-568-conjugated secondary antibody (1 : 5000; Molecular Probes) at room temperature for 90 min. Then they were counterstained with 2 μg/mL TO-PRO-3 (Molecular Probes) at room temperature for 10 min, and mounted in Gelvatol. A confocal laser scanning microscope (MRC1024; Bio-Rad Laboratories) was used for the morphological analysis.

Quantitative assessment of mitochondrial impairment and cell death

To assess cell viability through mitochondrial impairment, we used the 3-(4,5-dimethyl-thiazol-2yl)-5-(3-carboxymethoxyphenyl)-2-(4-sulfophenyl)-2H-tetrazolium (MTS) assay with CellTiter 96 Aqueous one solution assay (Promega, Madison, WI, USA), as described previously (Takeuchi *et al.* 2002a). At each time point (0, 24 and 48 h) after transfection, MTS assays were carried out in six independent trials. Absorbance at 490 nm was measured in a multiple plate reader as described previously (Ishigaki *et al.* 2002).

Cell death was assessed by the dye exclusion method with propidium iodide (PI; Molecular Probes) as described previously (Takeuchi *et al.* 2002a). At each time point (0, 24 and 48 h) after transfection, cells were incubated with 2 μg/mL PI in DMEM for 15 min at room temperature and mounted in Gelvatol. More than 200 transfected cells in duplicate slides were assessed blindly in three independent trials under a conventional fluorescent microscope. The ratio of dead cells was calculated as a percentage of PI-positive cells among EGFP-positive cells.

Statistical analysis

All results were analyzed by two-way ANOVA with Tukey–Kramer post-hoc test, using Statview software version 5 (SAS Institute Inc., Cary, NC, USA).

Results

Dorfin reduces the levels of total, cytosolic and mitochondrial mutant SOD1

Confocal laser scanning microscopic images revealed that expression of both non-organelle-oriented Cyto-SOD1 plasmid and pcDNA3.1/HisMax-Dorfin was diffusely present in the cells. SOD1-EGFP fusion proteins were co-localized with Xpress-Dorfin fusion proteins (Figs 1a–i), consistent with our previous study (Niwa *et al.* 2002; Takeuchi *et al.* 2002a). In contrast, the expression of mitochondria-oriented Mito-SOD1 plasmid was observed in the mitochondria, as in our previous report (Takeuchi *et al.* 2002a), and was not co-localized with Xpress-Dorfin fusion proteins (Figs 1j–l). Western blots also revealed that Xpress-Dorfin fusion proteins were absent from the mitochondrial fraction (Fig. 1m). At 48 h after transfection, co-expression of Dorfin had reduced the total cell lysate level of SOD1-EGFP fusion proteins expressed by Cyto-G93A or Cyto-G85R by approximately 40%, whereas it did not affect those expressed by Cyto-WT (Fig. 2). In contrast, the amount of SOD1-EGFP fusion proteins expressed by Mito-SOD1 did not show any reduction even with co-expression of Dorfin (Fig. 2). In the cytosolic fraction, co-expression of Dorfin also reduced the level of SOD1-EGFP fusion proteins expressed by Cyto-G93A or Cyto-G85R by approximately 40%, whereas it did not affect those expressed by Cyto-WT (Fig. 3). As we described previously (Takeuchi *et al.* 2002a), cells with Mito-SOD1 showed very small amounts of SOD1-EGFP fusion proteins in the cytosolic fraction (Fig. 3). In the mitochondrial fraction, co-expression of Dorfin also reduced the level of SOD1-EGFP fusion proteins expressed by Cyto-G93A or Cyto-G85R by approximately 50%, whereas it did not affect those expressed by Cyto-WT (Fig. 4). This reduction in mitochondrial SOD1-EGFP was observed from 24 h after transfection, earlier than that of total or cytosolic SOD1-EGFP. In contrast, in the cells with Mito-SOD1, Dorfin did not reduce the amount of mitochondrial SOD1-EGFP fusion proteins (Fig. 4). The above results suggest that the mitochondrial accumulation of mutant SOD1 without organelle-oriented signals might be a result of mutant SOD1 in the cytosol, and we suggest that Dorfin, a cytosolic E3, reduced the accumulation of mutant SOD1 in the mitochondria by enhancing the degradation of mutant SOD1 in the cytosol, not in the mitochondria.

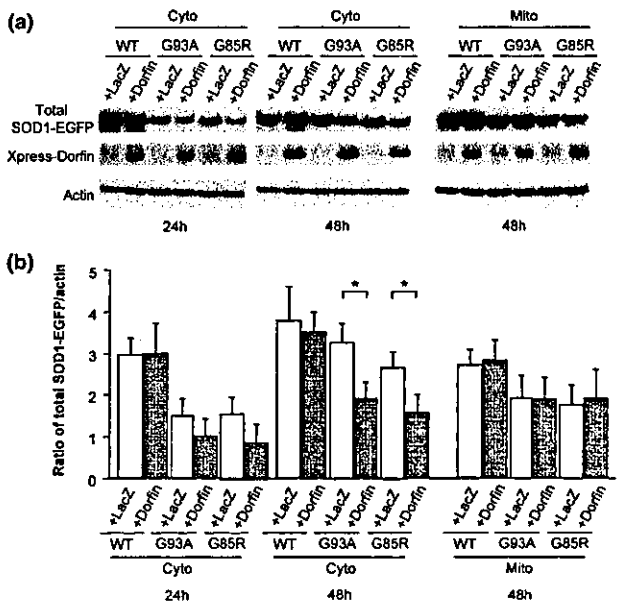

Fig. 2 Level of total SOD1-EGFP fusion protein. (a) Levels of total SOD1-EGFP fusion protein and Xpress-Dorfin fusion protein. (b) Densitometric analysis of total SOD1-EGFP fusion protein expressed as a ratio to actin. Dorfin significantly reduced the level of total SOD1-EGFP fusion protein expressed by Cyto-G93A or Cyto-G85R, whereas it did not reduce that expressed by Mito-SOD1. Values are mean ± SD ($n = 4$). *$p < 0.05$ (two-way ANOVA with Tukey–Kramer post-hoc test).

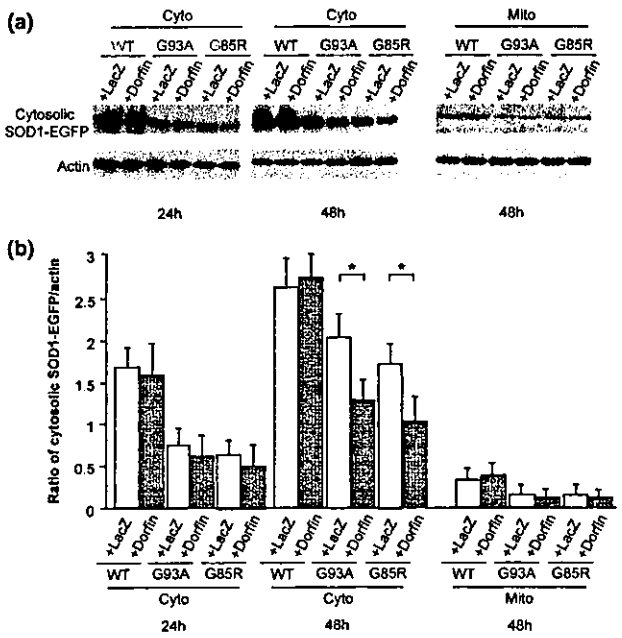

Fig. 3 Level of cytosolic SOD1-EGFP fusion protein. (a) Levels of cytosolic SOD1-EGFP fusion protein. (b) Densitometric analysis of cytosolic SOD1-EGFP fusion protein expressed as a ratio to actin. In the cytosolic fraction, Dorfin significantly reduced the levels of SOD1-EGFP fusion protein expressed by Cyto-G93A or Cyto-G85R. Mito-SOD1 showed very small amounts of SOD1-EGFP fusion proteins in the cytosolic fraction. Values are mean ± SD ($n = 4$). *$p < 0.05$ (two-way ANOVA with Tukey–Kramer post-hoc test).

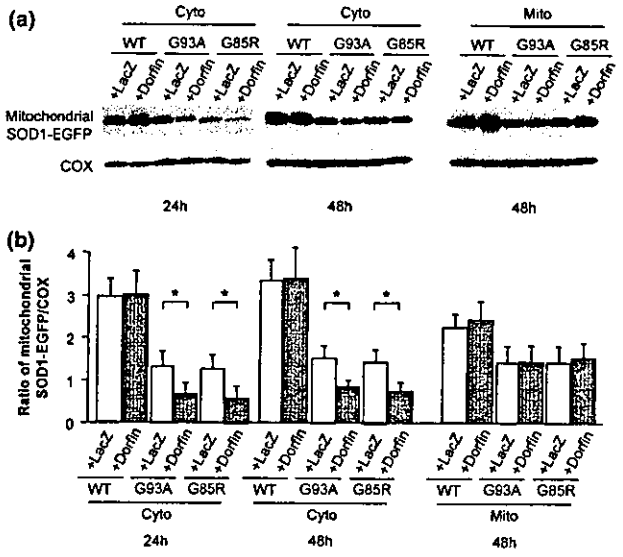

Fig. 4 Level of mitochondrial SOD1-EGFP fusion protein. (a) Levels of mitochondrial SOD1-EGFP fusion protein. (b) Densitometric analysis of mitochondrial SOD1-EGFP fusion protein expressed as a ratio to COX. In the mitochondrial fraction, Dorfin significantly reduced the level of SOD1-EGFP fusion protein expressed by Cyto-G93A or Cyto-G85R, whereas it did not reduce that expressed by Mito-SOD1. Values are mean ± SD ($n = 4$). $^*p < 0.05$ (two-way ANOVA with Tukey–Kramer post-hoc test).

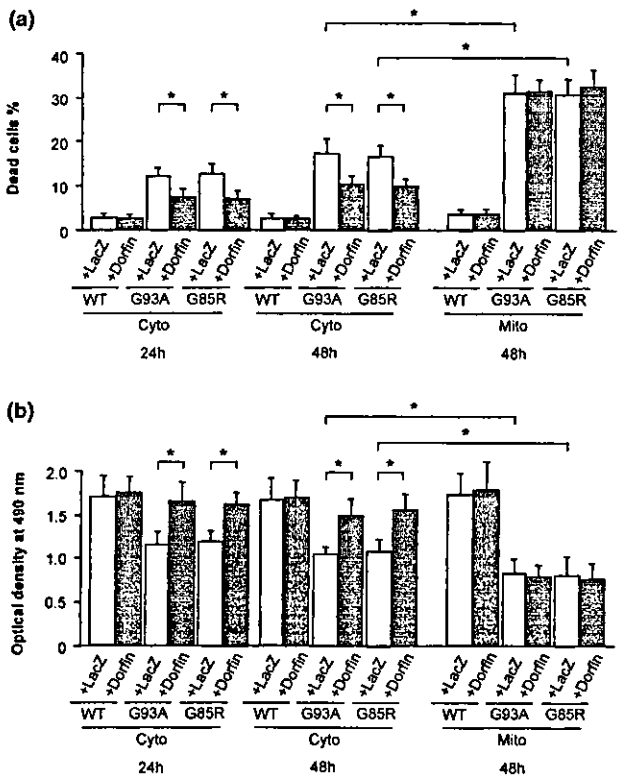

Fig. 5 (a) Frequency of dead cells and (b) mitochondrial impairment analyzed by MTS assay. The cells with Mito-G93A and Mito-G85R exhibited a significantly higher level of cell death and mitochondrial impairment than those with Cyto-G93A and Cyto-G85R. Dorfin significantly decreased cell death and mitochondrial impairment induced by Cyto-G93A and Cyto-G85R, whereas it did not affect those induced by Mito-SOD1. Values are mean ± SD ($n = 6$). $^*p < 0.05$ (two-way ANOVA with Tukey–Kramer post-hoc test).

Dorfin protects neuronal cells from mutant SOD1-mediated neurotoxicity by reducing mitochondrial mutant SOD1

As we demonstrated previously (Takeuchi *et al.* 2002a), the cells with Cyto-G93A and Cyto-G85R underwent cell death (Fig. 5a) and mitochondrial impairment (Fig. 5b), whereas those with Cyto-WT did not. The cells with Mito-G93A and Mito-G85R exhibited significantly more cell death and mitochondrial impairment than those with Cyto-G93A and Cyto-G85R, whereas those with Mito-WT did not (Fig. 5). Co-expression of Dorfin significantly ameliorated cell death and mitochondrial impairment induced by Cyto-G93A and Cyto-G85R (Fig. 5), as in our previous report (Niwa *et al.* 2002). In contrast, Dorfin did not affect cell death and mitochondrial impairment induced by Mito-SOD1 (Fig. 5), whose protein level Dorfin did not reduce. These findings suggest that Dorfin ameliorates mutant SOD1-mediated neurotoxicity by reducing the accumulation of mutant SOD1 in the mitochondria.

Dorfin reduces mitochondrial cytochrome *c* release and sequential activation of caspase-9 and caspase-3

We next assessed whether Dorfin reduced the mitochondrial death signal associated with the mutant SOD1-mediated cytotoxicity. Western blots revealed that Cyto-G93A and Cyto-G85R induced a gradual increase in the cytochrome *c* released from the mitochondria into the cytosol, whereas Cyto-WT did not (Fig. 6). The cells with Mito-G93A and Mito-G85R also exhibited a higher level of cytochrome *c* release than those with Cyto-G93A and Cyto-G85R, whereas those with Mito-WT did not (Fig. 6). Co-expression of Dorfin significantly reduced the release of cytochrome *c* from the mitochondria into the cytosol induced by Cyto-G93A and Cyto-G85R (Fig. 6). In the cells with Mito-G93A and Mito-G85R, however, Dorfin did not reduce the cytochrome *c* release from the mitochondria into the cytosol (Fig. 6).

Next, we examined whether Dorfin affected the downstream signal cascade of the activation of caspase-9 and caspase-3 following the release of mitochondrial cytochrome *c*. As we demonstrated previously (Takeuchi *et al.* 2002a), western blots revealed that Cyto-G93A and Cyto-G85R induced gradual activation of caspase-9 and caspase-3, whereas Cyto-WT did not (Figs 7 and 8). The cells with Mito-G93A and Mito-G85R exhibited a higher level of activation of caspase-9 and caspase-3 than those with Cyto-G93A and Cyto-G85R, whereas those with Mito-WT did not (Figs 7 and 8). Co-expression of Dorfin significantly reduced

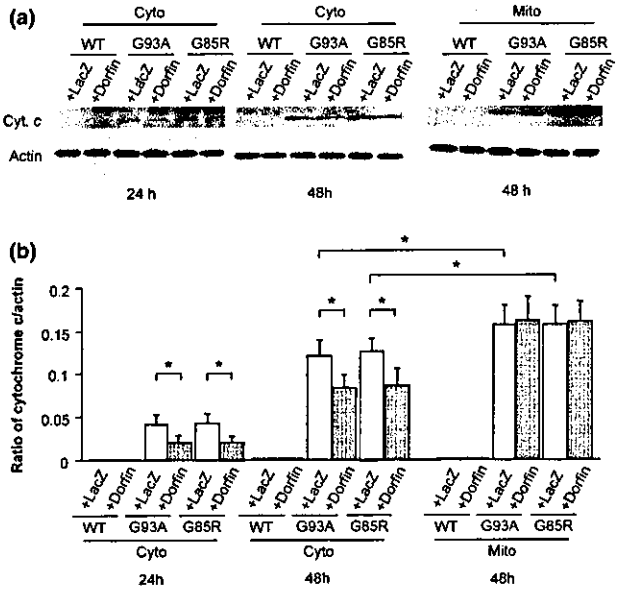

Fig. 6 Western blot analysis of cytochrome *c* release. (a) Time course of mitochondrial cytochrome *c* release into the cytosol. (b) Densitometric analysis of cytochrome *c* release expressed as a ratio to COX. The cells with Mito-G93A and Mito-G85R exhibited significantly more cytochrome *c* release than those with Cyto-G93A and Cyto-G85R. Dorfin significantly reduced the amount of mitochondrial cytochrome *c* released into the cytosol induced by Cyto-G93A and Cyto-G85R, whereas it did not affect that induced by Mito-SOD1. Values are mean ± SD ($n = 4$). $^*p < 0.05$ (two-way ANOVA with Tukey–Kramer post-hoc test).

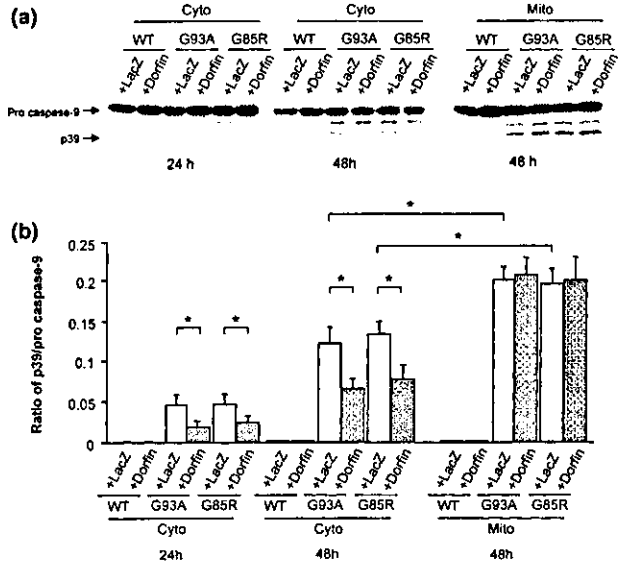

Fig. 7 Western blot analysis of caspase-9 activation. (a) Time course of the activation of caspase-9. (b) Densitometric analysis of caspase-9 activation. The cells with Mito-G93A and Mito-G85R exhibited significantly more activation of caspase-9 than those with Cyto-G93A and Cyto-G85R. Dorfin significantly reduced the activation of caspase-9 induced by Cyto-G93A and Cyto-G85R, whereas it did not reduce that induced by Mito-SOD1. Values are mean ± SD ($n = 4$). $^*p < 0.05$ (two-way ANOVA with Tukey–Kramer post-hoc test).

the activation of caspase-9 and caspase-3 induced by Cyto-G93A and Cyto-G85R (Figs 7 and 8). However, Dorfin did not reduce the activation of caspase-9 and caspase-3 induced by Mito-G93A and Mito-G85R (Figs 7 and 8), as it did not reduce the release of cytochrome *c* induced by Mito-G93A and Mito-G85R (Fig. 6). These findings combined with the aforementioned observations suggest that the reduction in the amount of mitochondrial mutant SOD1 due to Dorfin results in attenuated activation of the mitochondrial PCD pathway and prevents eventual cell death.

Discussion

In the present study, we first demonstrated that Dorfin, an E3 for mutant SOD1s, attenuated the activation of the mitochondrial PCD pathway and prevented eventual cell death in a neuronal cell model of FALS by reducing the amount of mutant SOD1 in the mitochondria. Dorfin reduced the levels of both cytosolic and mitochondrial mutant SOD1-EGFP fusion proteins that were expressed by Cyto-G93A and Cyto-G85R without organelle-oriented signals, whereas Dorfin did not affect the level of mutant SOD1-EGFP fusion protein that was expressed by Mito-G93A and Mito-G85R with mitochondrial localizing signals. The reduction in the level of

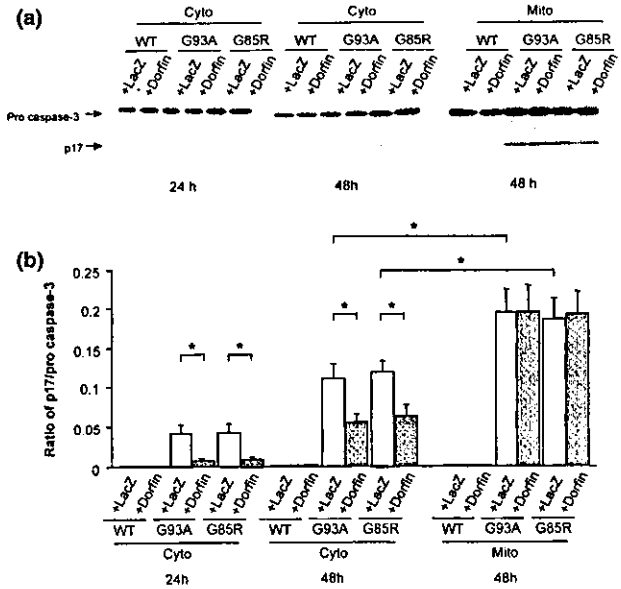

Fig. 8 Western blot analysis of caspase-3 activation. (a) Time course of activation of caspase-3. (b) Densitometric analysis of caspase-3 activation. The cells with Mito-G93A and Mito-G85R exhibited significantly more activation of caspase-3 than those with Cyto-G93A and Cyto-G85R. Dorfin significantly reduced the activation of caspase-3 induced by Cyto-G93A and Cyto-G85R, whereas it did not reduce that induced by Mito-SOD1. Values are mean ± SD ($n = 4$). $^*p < 0.05$ (two-way ANOVA with Tukey–Kramer post-hoc test).

mitochondrial SOD1-EGFP was observed earlier than that of total or cytosolic SOD1-EGFP. Moreover, Dorfin was present in the cytosol, not in the mitochondria. These findings indicated that the mitochondrial mutant SOD1 without organelle-oriented signals (Cyto-G93A and Cyto-G85R) might be translocated from the cytosol, and we suggest that Dorfin reduces the mitochondrial accumulation of mutant SOD1 by enhancing the degradation of mutant SOD1 in the cytosol through the ubiquitin–proteasomal pathway, thereby reducing the uptake of mutant SOD1 into the mitochondria.

Many reports have documented mitochondrial involvement in ALS and FALS. Mitochondrial degeneration with vacuolization or membrane disintegration in motor neurons is one of the earliest pathological findings in FALS Tg mice (Dal Canto and Gurney 1994; Wong *et al.* 1995; Hirano 1996; Kong and Xu 1998; Jaarsma *et al.* 2000; Higgins *et al.* 2003). Moreover, mitochondrial dysfunction such as altered calcium homeostasis (Carri *et al.* 1997; Menzies *et al.* 2002b), decreased respiratory chain complex activity (Mattiazzi *et al.* 2002; Menzies *et al.* 2002a), alteration of mitochondria-related gene expression (Yoshihara *et al.* 2002) and an increase in reactive oxygen species (Beretta *et al.* 2003) have been reported in *in vitro* and *in vivo* models of FALS. Several studies have documented that SOD1, which has been considered a cytosolic enzyme, also exists in the mitochondrial intermembrane space (Okado-Matsumoto and Fridovich 2001; Sturtz *et al.* 2001; Higgins *et al.* 2002) and that the mitochondrial vacuoles are lined with mutant SOD1 in a FALS Tg mice model (Jaarsma *et al.* 2001; Higgins *et al.* 2003). Although the mitochondria-oriented vector we used here is designed to localize proteins to the mitochondrial matrix, we predict that SOD1-EGFP also exists in the mitochondrial intermembrane space through the process of its uptake into the mitochondrial matrix in our model, although were not able to confirm this. Recent studies also revealed that SOD1 in the mitochondria originates from the uptake of SOD1 in the cytosol (Sturtz *et al.* 2001; Okado-Matsumoto and Fridovich 2002; Field *et al.* 2003). At least our result provided enough evidence that Dorfin interacts with mutant SOD1 in the cytosol, not in the mitochondria. Thus we suggest that Dorfin indirectly reduces the mitochondrial accumulation of mutant SOD1 by reducing the uptake of mutant SOD1 into the mitochondria.

Previous studies demonstrated that the mitochondrial PCD pathway, cytochrome *c* release and subsequent caspase activation, might contribute to the motor neuron cell death in FALS (Durham *et al.* 1997; Martin 1999; Li *et al.* 2000; Pasinelli *et al.* 2000; Guégan *et al.* 2001; Kriz *et al.* 2002; Zhu *et al.* 2002). Thus, inhibiting the activation of the mitochondrial PCD pathway is potentially useful in the treatment of FALS. Methods for this include inhibition of cytochrome *c* release by minocycline (Zhu *et al.* 2002; Kriz *et al.* 2002), co-expression of bcl-2 (Lee *et al.* 2001) or X-chromosome-linked inhibitor of apoptosis protein (Ishigaki *et al.* 2002), and treatment with a broad caspase inhibitor zVAD-fmk (Pasinelli *et al.* 2000; Takeuchi *et al.* 2002a) or a caspase-9 specific inhibitor zLEHD-fmk (Takeuchi *et al.* 2002a). In this study, we demonstrated that Dorfin reduces the amount of mitochondrial mutant SOD1, attenuates the activation of the mitochondrial PCD pathway and prevents eventual neuronal cell death. It is therefore possible that reducing the amount of mutant SOD1 in the mitochondria may be adopted as a new therapeutic strategy for mutant SOD1-associated FALS.

Recent studies have suggested that some E3s, including Dorfin, act in a quality-control system to degrade cytosolic or transmembranous unfolded abnormal proteins (Moynihan *et al.* 1999; Fang *et al.* 2001; Meacham *et al.* 2001; Murata *et al.* 2001; Yoshida *et al.* 2002). The mitochondria also have a quality-control system that depends on mitochondria-specific molecular chaperones and ATPases associated with diverse cellular activities (AAA) proteases such as chaperonin 60 (Gottesman *et al.* 1997), mitochondrial heat-shock protein 70 (Savel'ev *et al.* 1998), and homologs of Lon, Yme1p, ClpP and ClpX (Wang *et al.* 1993; Suzuki *et al.* 1997; Langer 2000; Shah *et al.* 2000; Kang *et al.* 2002; Röttgers *et al.* 2003). A recent study documented that the accumulation of unfolded abnormal proteins in the mitochondria itself up-regulated the nuclear gene expression encoding mitochondrial-specific molecular chaperones (Zhao *et al.* 2002). Even though the mitochondria are able to dispose of abnormal proteins, they appear to have limited capacity to do this. They also seem to release death signals when abnormal proteins overflow their disposing capacity. Combination therapy such as Dorfin and mitochondria-specific molecular chaperones or AAA proteases thus seems more effective. Further investigations are needed to develop this therapeutic avenue.

There remains the problem of how the mutant SOD1 induces the mitochondrial PCD pathway. One of our previous studies revealed that bcl-2 family pro-apoptotic proteins, such as Bax, Bak, Bid, Bad and Bim, and other mitochondrial death signals such as apoptosis-inducing factor (AIF) and second mitochondria-derived activator of caspase (Smac) were not involved in the neuronal cell death in our model (Takeuchi *et al.* 2002a). Other studies have reported that translocation of Bax and cleavage of Bid were associated with neuronal cell death in the FALS Tg mouse model (Guégan *et al.* 2001; 2002), but there is a possibility that the surrounding environment of motor neurons such as astrocytes, microglia or dying neurons might have been affected in these models. Moreover, we have indicated that a non-apoptotic form of PCD might contribute to neuronal cell death through the mitochondrial PCD pathway in our model (Takeuchi *et al.* 2002a). Another report also mentioned that a non-apoptotic type of PCD acting through the mitochondrial PCD pathway might underlie mutant SOD1-related neurotoxicity (Guégan and Przedborski 2003). Further *in vivo*

investigations are needed to shed light on the mechanism of mutant SOD1-mediated neuronal cell death.

In this study we demonstrated that Dorfin, an E3 for mutant SOD1s, significantly reduced the level of mutant SOD1 in the mitochondria, attenuated the subsequent activation of the mitochondrial PCD pathway and prevented eventual neuronal cell death in a neuronal cell model of FALS. Reducing the accumulation of mutant SOD1 in the mitochondria may have an important place in the therapeutic strategy for mutant SOD1-associated FALS, and Dorfin may play a key role in this.

Acknowledgements

We are grateful to Dr Keiji Tanaka (Department of Molecular Oncology, The Tokyo Metropolitan Institute of Medical Science) for his helpful comments. This work was supported by grants from the Ministry of Health, Labor and Welfare of Japan, and a Center of Excellence grant from the Ministry of Education, Culture, Sports, Science and Technology of Japan.

References

Ardley H. C., Tan N. G. S., Rose S. A., Markham A. F. and Robinson P. A. (2001) Features of the Parkin/Ariadne-like ubiquitin ligase, HHARI, that regulate its interaction with the ubiquitin-conjugating enzyme, UbcH7. *J. Biol. Chem.* **276**, 19640–19647.

Beretta S., Sala G., Mattavelli L., Ceresa C., Casciati A., Ferri A., Carr ı M. T. and Ferrarese C. (2003) Mitochondrial dysfunction due to mutant copper/zinc superoxide dismutase associated with amyotrophic lateral sclerosis is reversed by *N*-acetylcysteine. *Neurobiol. Dis.* **13**, 213–221.

Carri M. T., Ferri A., Battistoni A., Famhy L., Gabbianelli R., Poccia F. and Rotilio G. (1997) Expression of a Cu,Zn superoxide dismutase typical of familial amyotrophic lateral sclerosis induces mitochondrial alteration and increase of cytosolic Ca^{2+} concentration in transfected neuroblastoma SH-SY5Y cells. *FEBS Lett.* **414**, 365–368.

Dal Canto M. C. and Gurney M. E. (1994) Development of central nervous system pathology in a murine transgenic model of human amyotrophic lateral sclerosis. *Am. J. Pathol.* **145**, 1271–1279.

Durham H. D., Roy J., Dong L. and Figlewic Z. D. A. (1997) Aggregation of mutant Cu/Zn superoxide dismutase proteins in a culture model of ALS. *J. Neuropathol. Exp. Neurol.* **56**, 523–530.

Fang S., Ferrone M., Yang C., Jensen J. P., Tiwari S. and Weissman A. M. (2001) The tumor autocrine motility factor receptor, gp78, is a ubiquitin protein ligase implicated in degradation from the endoplasmic reticulum. *Proc. Natl Acad. Sci. USA* **98**, 14422–14427.

Field L. S., Furukawa Y., O'Halloran T. V. and Culotta V. C. (2003) Factors controlling the uptake of yeast Cu/Zn superoxide dismutase into mitochondria. *J. Biol. Chem.* **278**, 28052–28059.

Gottesman S., Wickner S. and Maurizi M. R. (1997) Protein quality control: triage by chaperones and proteases. *Genes Dev.* **11**, 815–823.

Guégan C. and Przedborski S. (2003) Programmed cell death in amyotrophic lateral sclerosis. *J. Clin. Invest.* **111**, 153–161.

Guégan C., Vila M., Rosoklija G., Hays A. P. and Przedborski S. (2001) Recruitment of the mitochondrial-dependent apoptotic pathway in amyotrophic lateral sclerosis. *J. Neurosci.* **21**, 6569–6576.

Guégan C., Vila M., Teissman P., Chen C., Onténiente B., Li M., Friedlander R. M. and Przedborski S. (2002) Instrumental activation of Bid by caspase-1 in a transgenic mouse model of ALS. *Mol. Cell. Neurosci.* **20**, 553–562.

Higgins C. M., Jung C., Ding H. and Xu Z. (2002) Mutant Cu,Zn superoxide dismutase that causes motoneuron degeneration is present in mitochondria in the CNS. *J. Neurosci.* **22 RC215**.

Higgins C. M. J., Jung C. and Xu Z. (2003) ALS-associated mutant SOD1G93A causes mitochondrial vacuolation by expansion of the intermembrane space and by involvement of SOD1 aggregation and peroxisomes. *BMC Neurosci.* **4**, 16–29.

Hirano A. (1996) Neuropathology of ALS: an overview. *Neurology* **47**, S63–S66.

Ishigaki S., Liang Y., Yamamoto M., Niwa J., Ando Y., Yoshihara T., Takeuchi H., Doyu M. and Sobue G. (2002) X-linked inhibitor of apoptosis protein is involved in mutant SOD1-mediated neuronal degeneration. *J. Neurochem.* **82**, 576–584.

Jaarsma D., Haasdijk E. D., Grashorn J. A. C., Hawkins R., van Duijn W., Verspaget H. W., London J. and Holstege J. C. (2000) Human Cu/Zn superoxide dismutase (SOD1) overexpression in mice causes mitochondrial vacuolization, axonal degeneration, and premature motoneuron death and accelerates motoneuron disease in mice expressing a familial amyotrophic lateral sclerosis mutant SOD1. *Neurobiol. Dis.* **7**, 623–643.

Jaarsma D., Rognoni F., van Duijn W., Verspaget H. W., Haasdijk E. D. and Holstege J. C. (2001) CuZn superoxide dismutase (SOD1) accumulates in vacuolated mitochondria in transgenic mice expressing amyotrophic lateral sclerosis-linked SOD1 mutations. *Acta Neuropathol.* **102**, 293–305.

Kang S. G., Ortega J., Singh S. K., Wang N., Huang N., Steven A. C. and Maurizi M. R. (2002) Functional proteolytic complexes of the human mitochondrial ATP-dependent protease, hClpXP. *J. Biol. Chem.* **277**, 21095–21102.

Kong J. and Xu Z. (1998) Massive mitochondrial degeneration in motor neurons triggers the onset of amyotrophic lateral sclerosis in mice expressing a mutant SOD1. *J. Neurosci.* **18**, 3241–3250.

Kriz J., Nguyen M. D. and Julien J. P. (2002) Minocycline slows disease progression in a mouse model of amyotrophic lateral sclerosis. *Neurobiol. Dis.* **10**, 268–278.

Langer T. (2000) AAA proteases: cellular machines for degrading membrane proteins. *Trends Biochem. Sci.* **25**, 247–251.

Lee M. H., Hyun D.-H., Halliwell B. and Jenner P. (2001) Effect of overexpression of wild-type and mutant Cu/Zn-superoxide dismutases on oxidative stress and cell death induced by hydrogen peroxide, 4-hydroxynonenal or serum deprivation: potentiation of injury by ALS-related mutant superoxide dismutases and protection by Bcl-2. *J. Neurochem.* **78**, 209–220.

Li M., Ona V. O., Guégan C. *et al.* (2000) Functional role of caspase-1 and caspase-3 in an ALS transgenic mouse model. *Science* **288**, 335–339.

Martin L. J. (1999) Neuronal death in amyotrophic lateral sclerosis is apoptosis: possible contribution of a programmed cell death mechanism. *J. Neuropathol. Exp. Neurol.* **58**, 459–471.

Mattiazzi M., D'Aurelio M., Gajewski C. D., Martushova K., Kiaei M., Beal M. F. and Manfredi G. (2002) Mutated human SOD1 causes dysfunction of oxidative phosphorylation in mitochondria of transgenic mice. *J. Biol. Chem.* **277**, 29626–29633.

Meacham G. C., Patterson C., Zhang W., Younger J. M. and Cyr D. M. (2001) The Hsc70 co-chaperone CHIP targets immature CFTR for proteasomal degradation. *Nat. Cell Biol.* **3**, 100–105.

Menzies F. M., Cookson M. R., Taylor R. W., Turnbull D. M., Chrzanowska-Lightowlers Z. M., Dong L., Figlewicz D. A. and Shaw P. J. (2002a) Mitochondrial dysfunction in a cell culture model of familial amyotrophic lateral sclerosis. *Brain* **125**, 1522–1533.

Menzies F. M., Ince P. G. and Shaw P. J. (2002b) Mitochondrial involvement in amyotrophic lateral sclerosis. *Neurochem. Int.* **40**, 543–551.

Moynihan T. P., Ardley H. C., Nuber U., Rose S. A., Jones P. F., Markham A. F., Scheffner M. and Robinson P. A. (1999) The ubiquitin-conjugating enzymes UbcH7 and UbcH8 interact with RING finger/IBR motif-containing domains of HHARI and H7-AP1. *J. Biol. Chem.* **274**, 30963–30968.

Murata S., Minami Y., Minami M., Chiba T. and Tanaka K. (2001) CHIP is a chaperone-dependent E3 ligase that ubiquitylates unfolded protein. *EMBO Report* **2**, 1133–1138.

Niwa J., Ishigaki S., Doyu M., Suzuki T., Tanaka K. and Sobue G. (2001) A novel centrisomal RING-finger protein, Dorfin, mediates ubiquitin ligase activity. *Biochem. Biophys. Res. Commun.* **281**, 706–713.

Niwa J., Ishigaki S., Hishikawa N., Yamamoto M., Doyu M., Murata S., Tanaka K., Taniguchi N. and Sobue G. (2002) Dorfin ubiquitylates mutant SOD1 and prevents mutant SOD1-mediated neurotoxicity. *J. Biol. Chem.* **277**, 36793–36798.

Okado-Matsumoto A. and Fridovich I. (2001) Subcellular distribution of superoxide dismutase (SOD) in rat liver. *J. Biol. Chem.* **276**, 38388–38393.

Okado-Matsumoto A. and Fridovich I. (2002) Amyotrophic lateral sclerosis: a proposed mechanism. *Proc. Natl Acad. Sci. USA* **99**, 9010–9014.

Pasinelli P., Houseweart M. K., Brown R. H. Jr and Cleveland D. W. (2000) Caspse-1 and -3 are sequentially activated in motor neuron death in Cu,Zn superoxide dismutase-mediated familial amyotrophic lateral sclerosis. *Proc. Natl Acad. Sci. USA* **97**, 13901–13906.

Raoul C., Estévez A. G., Nishimune H., Cleveland D. W., deLapeyrière O., Henderson C. E., Haase G. and Pettmann B. (2002) Motoneuron death triggered by a specific pathway downstream of Fas; potentiation by ALS-linked SOD1 mutations. *Neuron* **35**, 1067–1083.

Rosen D. R., Siddique T., Patterson D. *et al.* (1993) Mutations in Cu/Zn superoxide dismutase gene are associated with familial amyotrophic lateral sclerosis. *Nature* **362**, 59–62.

Röttgers K., Zufall N., Guiard B. and Voos W. (2003) The ClpB homolog Hsp78 is required for the efficient degradation of proteins in the mitochondrial matrix. *J. Biol. Chem.* **277**, 45829–45837.

Savel'ev A. S., Novikova L. A., Kovaleva I. E., Luzikov V. N., Neupert W. and Langer T. (1998) ATP-dependent proteolysis in mitochondria. *J. Biol. Chem.* **273**, 20596–20602.

Shah Z. H., Hakkaart G. A. J., Arku B., de Jong L., van der Spek H., Grivell L. A. and Jacobs H. T. (2000) The human homologue of the yeast mitochondrial AAA metalloprotease Yme1p complements a yeast *yme1* disruptant. *FEBS Lett.* **478**, 267–270.

Sturtz L. A., Diekert K., Jensen L. T., Lill R. and Culotta V. C. (2001) A fraction of yeast Cu,Zn-superoxide dismutase and its metallochaperone, CCS, localize to the intermembrane space of mitochondria. *J. Biol. Chem.* **276**, 38084–38089.

Suzuki C. K., Rep M., van Dijl J. M., Suda K., Grivell L. A. and Schatz G. (1997) ATP-dependent proteases that also chaperone protein biogenesis. *Trends Biochem. Sci.* **22**, 118–123.

Takeuchi H., Kobayashi Y., Ishigaki S., Doyu N. and Sobue G. (2002a) Mitochondrial localization of mutant superoxide dismutase 1 triggers caspase-dependent cell death in a cellular model of familial amyotrophic lateral sclerosis. *J. Biol. Chem.* **277**, 50966–50972.

Takeuchi H., Kobayashi Y., Yoshihara T., Niwa J., Doyu M., Ohtsuka K. and Sobue G. (2002b) Hsp70 and Hsp40 improve neurite outgrowth and suppress intracytoplasmic aggregate formation in cultured neuronal cells expressing mutant SOD1. *Brain Res.* **949**, 11–22.

Wang N., Gottesman S., Willingham M. C., Gottesman M. M. and Maurizi M. R. (1993) A human mitochondrial ATP-dependent protease that is highly homologous to bacterial Lon protease. *Proc. Natl Acad. Sci. USA* **90**, 11247–11251.

Wong P. C., Pardo C. A., Borchelt D. R., Lee M. K., Copeland N. G., Jenkins N. A., Sisodia S. S., Cleveland D. W. and Price D. L. (1995) An adverse property of a familial ALS-linked SOD1 mutation causes motor neuron disease characterized by vacuolar degeneration of mitochondria. *Neuron* **14**, 1105–1116.

Yim M. B., Kang J. H., Yim H. S., Kwak H. S., Chock P. B. and Stadtman E. R. (1996) A gain-of-function of an amyotrophic lateral sclerosis-associated Cu,Zn-superoxide dismutase mutant: an enhancement of free radical formation due to a decrease in K_m for hydrogen peroxide. *Proc. Natl Acad. Sci. USA* **93**, 5709–5714.

Yoshida Y., Chiba T., Tokunaga F. *et al.* (2002) E3 ubiquitin ligase that recognizes sugar chains. *Nature* **418**, 438–442.

Yoshihara T., Ishigaki S., Yamamoto M., Liang Y., Niwa J., Takeuchi H., Doyu M. and Sobue G. (2002) Differential expression of inflammation- and apoptosis-related genes in spinal cords of a mutant SOD1 transgenic mouse model of familial lateral sclerosis. *J. Neurochem.* **80**, 158–167.

Zhao Q., Wang J., Levichkin I. V., Stasinopoulos S., Ryan M. T. and Hoogenraad N. J. (2002) A mitochondrial specific stress response in mammalian cells. *EMBO J.* **21**, 4411–4419.

Zhu S., Stavrovskaya I. G., Drozda M. *et al.* (2002) Minocycline inhibits cytochrome *c* release and delays progression of amyotrophic lateral sclerosis. *Nature* **417**, 74–78.

Pathology of early- vs late-onset TTR Met30 familial amyloid polyneuropathy

H. Koike, MD, PhD; K. Misu, MD, PhD; M. Sugiura, MD; M. Iijima, MD; K. Mori, MD, PhD; M. Yamamoto, MD, PhD; N. Hattori, MD, PhD; E. Mukai, MD, PhD; Y. Ando, MD, PhD; S. Ikeda, MD, PhD; and G. Sobue, MD, PhD

Abstract—*Background:* Late-onset type I familial amyloid polyneuropathy (FAP TTR Met30) cases unrelated to endemic foci in Japan show clinical features setting them apart from early-onset cases in endemic foci. *Objective:* To compare pathologic features between the early- and late-onset types. *Methods:* Pathologic findings in FAP TTR Met30 with onset before age 50 in relation to endemic foci (11 cases) were compared with those in 11 later-onset cases unrelated to endemic foci. *Results:* Sural nerve biopsy specimens showed predominantly small-fiber loss in early-onset cases; variable fiber size distribution, axonal sprouting, and relatively preserved unmyelinated fibers characterized late-onset cases. Autopsy cases representing both groups showed amyloid deposition throughout the length of nerves and in sympathetic and sensory ganglia, but amounts were greater in early-onset cases. Amyloid deposition and neuronal cell loss were greater in sympathetic than dorsal root ganglia in early-onset cases; the opposite was true in late-onset cases. Size assessment of remaining neurons in these ganglia suggested predominant loss of small neurons in early-onset cases but loss of neurons of all sizes in late-onset cases. Transthyretin-positive, Congo red-negative amorphous material was more conspicuous in nerves from late- than early-onset cases. In extraneural sites, amyloid was more conspicuous in thyroid and kidney from early-onset cases and in heart and hypophysis from late-onset cases. In early-onset cases, cardiac amyloid deposition was prominent in the atrium and subendocardium but was conspicuous throughout the myocardium in late-onset cases. *Conclusion:* The pathology of early- and late-onset FAP TTR Met30 correlated well with differences in clinical findings.

NEUROLOGY 2004;63:129–138

Familial amyloid polyneuropathy type I (transthyretin Met30-associated familial amyloid polyneuropathy; FAP TTR Met30), in which methionine is substituted for valine at position 30 of transthyretin, is the most common type of FAP in Japan as well as in Western countries.[1-6] In Japan, cases have been particularly concentrated in two geographic areas: the village of Ogawa in Nagano Prefecture on the island of Honshu and the city of Arao in Kumamoto Prefecture on the island of Kyushu.[3,4] Although there are exceptions, typical cases of FAP TTR Met30 in these two endemic foci are characterized by early age at onset (second or third decade), a high penetrance rate, marked autonomic dysfunction, selective loss of superficial sensation including nociception and thermal sensation, atrioventricular conduction block requiring pacemaker implantation, steady progression of disease over 10 to 15 years, and presence of anticipation concerning age at onset.[3,4,7-11]

In contrast to these early-onset FAP TTR Met30 cases in endemic foci, we have reported the presence of a late-onset type of FAP TTR Met30 in a wide distribution throughout Japan.[9,10,12] Features of these cases were distinct from those of early-onset cases related to endemic foci. These differences included onset at ages over 50 years, a low penetrance rate, relatively mild autonomic dysfunction, loss of all sensory modalities rather than sensory dissociation, frequent presence of cardiomegaly, extreme male preponderance, and absence of anticipation concerning age at onset.[9,10,12] These geographic and clinical differences were confirmed in a subsequent nationwide survey.[11] Similar geographic and clinical contrasts between early- and late-onset types of FAP TTR Met30 have been reported in Portugal,[1,5,13] although not in the form of a large-scale comparative study.

The reasons for contrasting features in early- and late-onset FAP with the same mutation in the transthyretin gene have not yet been determined. In the current study, we investigated pathologic features of Japanese patients with early- and late-onset FAP TTR Met30, seeking explanations for the clinical differences.

Patients and methods. Pathologic findings were compared between consecutive patients with early- and late-onset FAP TTR Met30 who attended the Nagoya University Graduate School of Medicine for sural nerve biopsy or autopsy from 1989 to 2003. Inclusion criteria for early-onset cases were FAP TTR Met30 with an onset age under 50 years and a relationship to one of the two Japanese endemic foci within the two most recent prior genera-

From the Department of Neurology (Drs. Koike, Misu, Sugiura, Iijima, Mori, Yamamoto, Hattori, and Sobue), Nagoya University Graduate School of Medicine, Department of Neurology (Dr. Mukai), Nagoya National Hospital, Department of Laboratory Medicine (Dr. Ando), Kumamoto University School of Medicine, and Third Department of Medicine (Dr. Ikeda), Shinshu University School of Medicine, Matsumoto, Japan.

Supported by grants from the Ministry of Health, Labor, and Welfare of Japan.

Received October 8, 2003. Accepted in final form February 23, 2004.

Address correspondence and reprint requests to Dr. G. Sobue, Department of Neurology, Nagoya University Graduate School of Medicine, Nagoya 466-8550, Japan; e-mail: sobueg@med.nagoya-u.ac.jp

Table 1 Background and clinical features of early- and late-onset FAP TTR Met30

Case no.	Sex	Age at onset/ death, y	Duration of illness until biopsy, y	Relationship to endemic foci	Family history	Initial symptom	Sensory dissociation	Cardiac involvement		Cause of death
								Cardiomegaly	Pacemaker implantation	
Early-onset group										
1	F	28/35	—	+	+	A	+	−	+	Sudden death
2	F	37/51	—	+	+	A	+	−	+	Pneumonia
3	M	24/41	3	+	+	A	+	−	−	Pneumonia
4	M	35	2.5	+	ND*	W	+	−	−	
5	F	33	6	+	+	P	−	−	+	
6	M	35	3	+	+	P	+	+	−	
7	M	36	2	+	+	A	+	−	−	
8	M	40	1	+	+	P	+	−	−	
9	M	28	1	+	+	P	+	−	−	
10	F	34	2	+	ND*	A	+	−	+	
11	F	41	3	+	+	A	−	−	+	
Late-onset group										
12	M	64/67	2	−	−	P	+	−	−	Lung cancer
13	M	62/68	3	−	−	P	+	+	−	Heart failure
14	M	52/62	3	−	−	P	−	+	−	Heart failure
15	M	67	2	−	+	P	−	−	−	
16	M	77	0.5	−	−	P, HF	−	+	−	
17	M	56	1	−	−	W	−	+	−	
18	M	61	3	−	−	P	−	+	−	
19	M	56	3	−	−	P	−	+	−	
20	M	58	0.6	−	−	P	−	+	−	
21	M	60	1.25	−	−	A	−	+	−	
22	M	61	5	−	−	P, W	−	−	−	

Cardiomegaly was assessed at the time of first referral to the hospital. No patient belonged to the same kindred as another.

* Fathers of Cases 4 and 10 were from Ogawa Village but died of nonneurologic disease when the patients were children. Statistical significance (early-vs late-onset group) was present in the items of sex ($p < 0.05$), age at onset ($p < 0.0001$), relationship to endemic foci ($p < 0.0001$), family history ($p < 0.0001$), sensory dissociation ($p < 0.01$), cardiomegaly ($p < 0.01$), and pacemaker implantation ($p < 0.05$). Statistical analyses were performed using the χ^2 test or the Mann–Whitney U test as appropriate.

FAP = familial amyloid polyneuropathy; + = present; − = absent; A = autonomic symptoms; W = weakness in the lower legs; P = paresthesia in the legs; HF = heart failure; ND = not determined.

tions. For late-onset cases, inclusion criteria were FAP TTR Met30 with an onset age over 50 years and no relationship to the endemic foci within the two most recent prior generations. To confirm the diagnosis of FAP TTR Met30, DNA analyses for mutation of the transthyretin gene were performed in all patients as described previously.[4,14,15] Informed consent was obtained, and all aspects of the study were approved by the Ethics Committee of Nagoya University Graduate School of Medicine.

Of the 22 patients included, 11 were in the early-onset group and the other 11 belonged to the late-onset group (table 1). No patient in the study belonged to the same kindred as another. Age at onset in the early-onset group was 33.9 ± 5.4 years and in the late-onset group 61.3 ± 6.7 years. Duration from onset of neuropathy to sural nerve biopsy was 2.6 ± 1.5 years in the early-onset group and 2.2 ± 1.4 years in the late-onset group (no significant difference). Duration from onset to death in autopsy cases was 12.7 ± 5.1 years for early-onset disease but only 6.3 ± 3.5 years in late-onset cases. Clinical features in the two groups of patients agreed well with previous descriptions.[3,9,11] In the early-onset group, half of the patients initially had autonomic symptoms, and most patients manifested more profound impairment of superficial than deep sensation (i.e., sensory dissociation). Pacemaker implantation was required in five patients, and the apparent cause of death in one case was sudden cardiac arrest. In the late-onset group, on the other hand, most patients initially manifested paresthesias or weakness in the legs rather than autonomic symptoms. Sensory dissociation was infrequent, and most patients manifested cardiac hypertrophy evident by chest radiography or echocardiography as opposed to atrioventricular conduction block in the early-onset group.

Sural nerve biopsy was performed in nine of the early-onset cases and all of the late-onset cases as described previously.[16-19] Specimens were divided into two portions. The first was fixed in 2.5% glutaraldehyde in 0.125 *M* cacodylate buffer (pH 7.4). Most of this part was embedded in epoxy resin for morphometric and ultrastructural study. Density of myelinated fibers was assessed in toluidine blue-stained semithin sections using a computer-assisted image analyzer (Luzex FS; Nikon, Tokyo, Japan); densities of small and large myelinated fibers were calculated as described previously.[17-19] Clusters of two or more small myelinated fibers enclosed by one basement membrane were considered an instance of axonal sprouting.[20-22] For electron microscopic study,

Table 2 Pathologic findings in sural nerve biopsy specimens

Case no.	MF density, no./mm²				Axonal sprouting of MF, no./mm²	UMF density, no./mm²	Segmental de/remyelination, %	Axonal degeneration, %	Amyloid deposition, %
	Large	Small	Total	Small/large					
Early onset									
3	0	0	0	—*	0	0	ND†	ND†	ND
4	13	13	26	—*	0	0	ND†	ND†	7
5	11	22	33	—*	0	216	8	25	1
6	23	0	23	—*	0	212	ND†	ND†	2
7	711	395	1,106	0.56	0	431	5	21	1
8	2,700	1,449	4,149	0.54	9	2,370	10	17	0+
9	2,015	1,515	3,530	0.75	18	3,663	6	26	0+
10	1,090	427	1,517	0.39	6	844	3	9	4
11	1,659	237	1,896	0.14	10	861	ND	ND	0+
Mean ± SD	914 ± 1,018	451 ± 608	1,364 ± 1,583	0.48 ± 0.23	5 ± 7	993 ± 1,305	6.4 ± 2.7	19.6 ± 6.9	
Controls, n = 3	3,495 ± 179	5,172 ± 528	8,666 ± 665	1.48 ± 0.11		30,104 ± 1,115	3.7 ± 5.5	0.4 ± 0.3	
Late onset									
12	79	487	566	6.16	79	2,370	17	20	0+
13	619	527	1,146	0.85	40	7,973	1	37	0
14	329	1,172	1,501	3.56	184	10,990	8	14	0+
15	66	13	79	—*	0	1,293	19	25	1
16	92	250	342	3.30	53	2,155	2	15	0+
17	461	1,831	2,292	3.97	250	7,111	13	27	1
18	0	2,423	2,423	—*	224	4,310	6	19	0
19	132	132	264	1.00	13	2,586	6	24	0+
20	514	355	869	0.69	26	1,795	4	37	0
21	1,304	1,212	2,516	0.93	105	14,438	6	26	0
22	66	277	343	4.20	40	431	ND†	ND†	1
Mean ± SD	333 ± 386	789 ± 776	1,122 ± 925	2.74 ± 1.95	92 ± 88	7,308 ± 5,417	8.2 ± 6.1	24.4 ± 8.0	
Controls, n = 4	2,891 ± 251	4,995 ± 333	7,886 ± 334	1.74 ± 0.22		29,748 ± 3,587	9.5 ± 6.2	1.9 ± 1.9	

Control values for each group were age matched. Statistical significance (early-vs late-onset group) was present in the items of small/large ($p < 0.05$), axonal sprouting of MF ($p < 0.01$), and UMF density ($p < 0.01$). Statistical analyses were performed using the Mann–Whitney *U* test.

* Populations of myelinated fibers were too small to determine the ratio.
† Teased fibers could not be obtained owing to depletion of myelinated fibers.

MF = myelinated fiber; UMF = unmyelinated fiber; ND = not determined; 0+ = <0.5%.

epoxy resin-embedded specimens were cut into ultrathin transverse sections and stained with uranyl acetate and lead citrate. To assess the density of unmyelinated fibers, electron microscopic photographs were taken at a magnification of 4,000× in a random fashion to cover the area of ultrathin sections as described previously.[17,19,21] Density of unmyelinated fibers was estimated from these electron micrographs. The remainder of the glutaraldehyde-fixed sample was processed for teased fiber study, in which microscopic observations were classified according to criteria described previously.[17,18,23,24] The second portion of the specimen was fixed in 10% formalin solution and embedded in paraffin. Sections were cut by routine methods and stained with hematoxylin and eosin, Congo red, the Klüver–Barrera method, and the Masson trichrome method. Seven sural nerve specimens were obtained from subjects with nonneurologic diseases at autopsy and examined in the same manner as age-matched control subjects (three cases for early-onset group, age 39.0 ± 7.8 years; four cases for late-onset group, age 62.3 ± 7.9 years).

Autopsy was performed in three early-onset cases and three late-onset cases. The nervous system including brain, spinal cord, ventral and dorsal roots, dorsal root ganglia from L3 to L5, and sympathetic ganglia was removed, as were the visceral organs. Tissues were fixed in 10% formalin solution, embedded in paraffin, cut, and stained as described for sural nerve specimens. In two of the early-onset and one of the late-onset cases, the median nerve from the axilla to the wrist and the sciatic/tibial nerve from the upper thigh to above the medial malleolus also were removed and fixed in 0.05 *M* phosphate buffer (pH 7.4) containing 1.5% glutaraldehyde and 3% formalin. After fixation, samples were taken every 4 cm along the nerves, embedded in paraffin or epoxy resin, cut, and stained as described for sural nerve specimens. Portions of the ventral and dorsal spinal roots were also fixed and processed in the same manner. Some of the quantitative aspects of the peripheral nervous system findings in Cases 2 and 3 were previously published.[18] Some descriptive pathologic findings in the peripheral nervous system in Cases 12 to 14 also were roughly described previously.[9]

Numbers and diameters of sympathetic ganglion neurons and

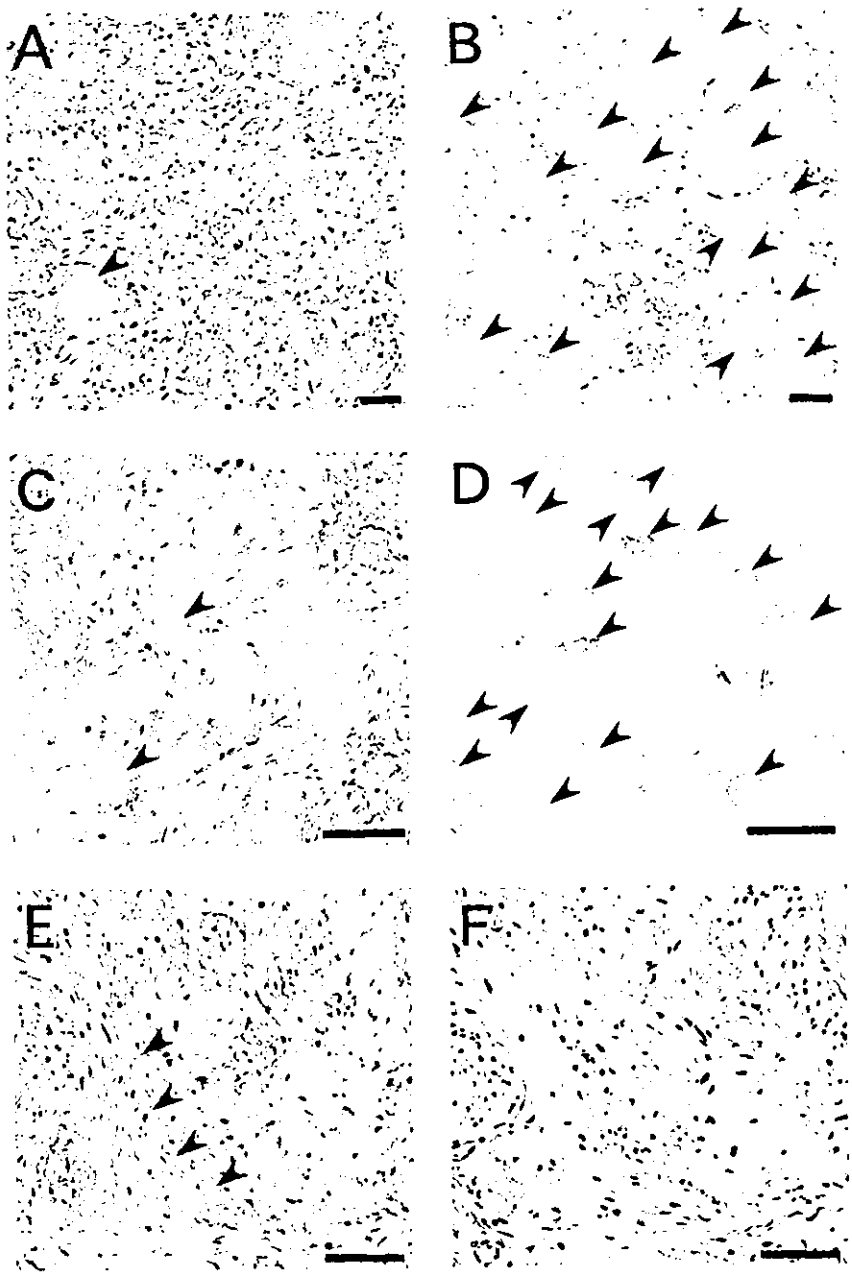

Figure 1. Representative postmortem findings in the peripheral nervous system. Amyloid deposits are identified by anti-human transthyretin antibody (A to E) or Congo red (F). (A, B) Dorsal root ganglia from early- and late-onset cases, respectively. (C, D) Sympathetic ganglia from early- and late-onset cases, respectively. In the dorsal root ganglia and sympathetic ganglia, amyloid deposition and neuronal cell loss are conspicuous in early-onset cases (A and C), whereas these are less severe in late-onset cases (B and D). Arrowheads indicate remaining neurons. (E, F) Consecutive specimens of the proximal part of sciatic nerve from a late-onset case. Amorphous material showing staining for transthyretin (E) but not with Congo red (F) is present in the subperineurial space (arrowheads). Bar = 40 μm.

dorsal root ganglion neurons were assessed using the image analyzer (Luzex FS). One hundred serial 10-μm-thick transverse sections at the middle portion of ganglia were prepared. Every tenth section was stained with the Klüver–Barrera method. Neurons showing obvious nucleoli in the sections were counted and measured to avoid split cell error. Number of neurons and area of ganglia on each section were assessed to calculate the density (neurons/mm^2). Values of neuronal cell density were expressed as means ± SD for these sections. For neuronal cell diameters, all neurons counted on 10 sections were measured. Values of neuronal cell diameter were expressed as means ± SD for these neurons. Control values for numbers and diameters of sympathetic and dorsal root ganglion neurons were obtained from four autopsy cases involving death from nonneurologic diseases.

Amounts of interstitial amyloid deposited in the parenchyma of various organs also were assessed using the Luzex FS analyzer. The proportion of area occupied by amyloid in each organ was determined as the extent of areas showing Congo red staining with emerald-green birefringence in polarized light and expressed as a percentage of the total transverse area. The proportion was assessed as the mean value for randomly selected areas covering at least 1 cm^2 of >10 sections. For nerve specimens, the proportion of area showing amyloid deposition to total endoneurial area was calculated. For the gastrointestinal tract, the proportion of area with amyloid deposition was assessed in the lamina muscularis mucosa.

Immunohistochemical assessment was performed with a peroxidase–antiperoxidase method using anti-human transthyretin antibody (Santa Cruz, CA) in consecutive deparaffinized sections.

Quantitative data, presented as means ± SD, were compared with control values. Statistical analyses were performed using the χ^2 test or the Mann–Whitney U test as appropriate. Values of p of <0.05 were considered to indicate significance.

Results. *Pathologic findings in sural nerve specimens.* In the early-onset cases, the density of large myelinated fibers was 914 ± 1,018 fibers/mm^2 (26% of age-matched normal control values) and that of small myelinated fibers was 451 ± 608 fibers/mm^2 (9% of age-matched normal control values), shown in table 2. Small myelinated fibers showed greater depletion than large myelinated fibers when myelinated fibers were not severely depleted overall (Cases 7 to 11). In late-onset cases, fiber size distribution

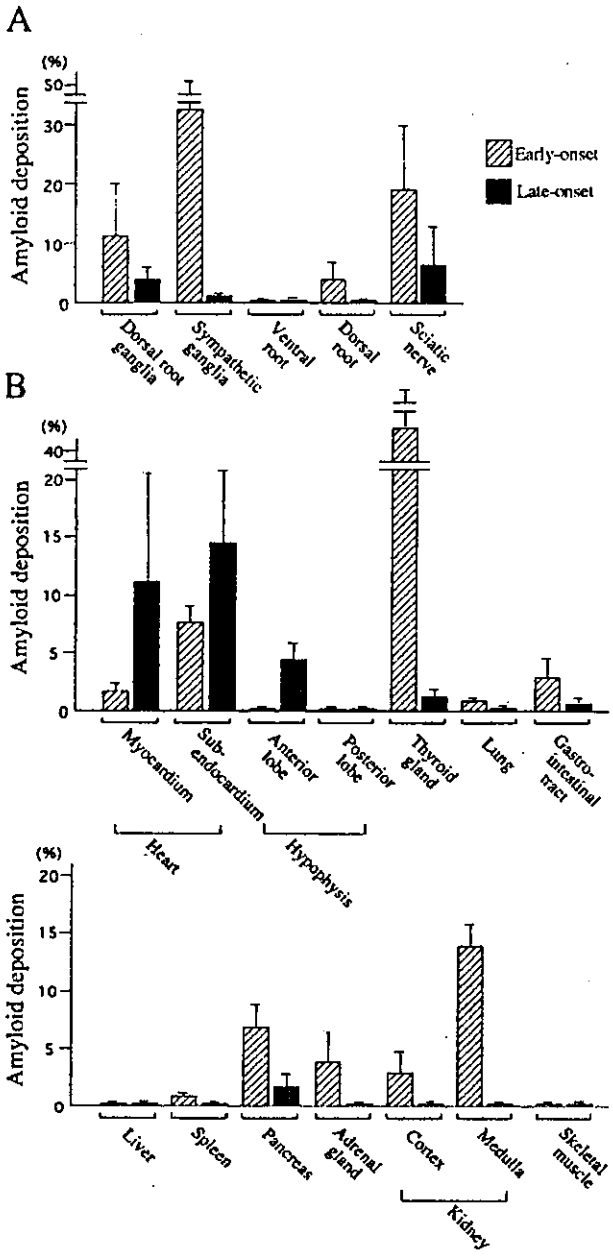

Figure 2. Amounts of interstitial amyloid deposited in the parenchyma of nervous system (A) and visceral organs (B). Hatched columns indicate mean values of early-onset cases (Cases 1 to 3), whereas filled columns indicate those of late-onset cases (Cases 12 to 14). Whiskers represent SDs. (A) Amyloid deposits in the nervous system are conspicuous in early-onset cases; these are less severe in late-onset cases. Amyloid deposition is more severe in sympathetic than dorsal root ganglia in early-onset cases, whereas the reverse pattern is seen in late-onset cases. (B) In early-onset cases, amyloid deposition is more prominent in the thyroid gland, gastrointestinal tract, pancreas, adrenal gland, and kidney than in late-onset cases. Amyloid deposition in early-onset cases is especially prominent in the thyroid gland and kidney, where deposition is scarce in late-onset cases. On the other hand, in late-onset cases, deposition is greater in the heart and anterior lobe of the hypophysis than in early-onset cases. Amyloid is scarce or absent in both groups in the posterior lobe of the pituitary gland, liver, and skeletal muscle.

of myelinated fibers, as indicated by the ratio of small to large myelinated fibers, was variable. Six cases (12, 14, 16 to 18, and 22) showed relative preservation of small myelinated fibers, whereas five cases (13, 15, 19 to 21) showed predominantly small-fiber loss as in early-onset cases. On average, density of large myelinated fibers was 333 ± 386 fibers/mm^2 (12% of age-matched normal control values) and that of small myelinated fibers was 789 ± 776 fibers/mm^2 (16% of age-matched normal control values). Axonal sprouting was scarce or absent in the early-onset group (5 ± 7/mm^2) but was relatively conspicuous in the late-onset group (92 ± 88/mm^2). Unmyelinated fibers were depleted more severely in the early- than the late-onset group (993 ± 1,305 vs 7,308 ± 5,417 fibers/mm^2; $p = 0.008$).

Amyloid deposition was scarce or absent in most cases in both groups, but relatively conspicuous deposition was observed in two of the early-onset cases (4 and 10). In both groups, amyloid was found in the endoneurium, both with and without relationship to small vessels.

Postmortem findings in the nervous system. Central nervous parenchyma was essentially intact in both groups, except that a small-cell carcinoma of the lung had metastasized to the cerebellum in Case 12, as previously described.[9,18] In the spinal cord, motor neurons as well as neurons in the Clarke columns were well preserved, and minimal to moderate myelinated fiber loss was observed in the posterior columns in both groups. Central chromatolysis was observed in spinal motor neurons in both groups. Amyloid deposits were not found in spinal cord parenchyma in any case.

In the dorsal root ganglia, amyloid deposits and neuronal cell loss were conspicuous in early-onset cases; these were less severe in late-onset cases (figures 1, A and B, and 2A). The mean diameter of remaining dorsal root ganglion neurons was larger in early-onset cases as compared with normal controls, suggesting predominant loss of small neurons (table 3). Mean neuronal cell diameters in late-onset cases were not notably different from those in normal controls, suggesting loss of neurons of all sizes. In the sympathetic ganglia, amyloid deposition and neuronal cell loss were very prominent in early-onset cases but less so in late-onset cases (see figures 1, C and D, and 2A). Size-selective neuronal cell loss was likely to be observed as in dorsal root ganglia (see table 3). Amyloid deposition and neuronal cell loss were more severe in sympathetic than dorsal root ganglia in early-onset cases, whereas the reverse pattern was seen in late-onset cases (see figure 2A and table 3). In the ventral spinal root, amyloid deposition was not apparent or only minimally present in both groups; likewise, myelinated fiber loss also was mild or not apparent in both groups. In the dorsal spinal root, amyloid deposition and myelinated fiber loss were moderately conspicuous in all early-onset cases but absent or minimal in late-onset cases. In sciatic and tibial nerves, amyloid deposition was more prominent in early-onset cases than the late-onset case (figure 3A). However, the late-onset case showed considerable myelinated fiber loss despite relative paucity of amyloid deposition (see figure 3B). In the median nerve, amyloid deposition also was more severe in early-onset cases than in the late-onset case, whereas myelinated fiber loss was more severe in the late-onset case than in early-onset cases. Amorphous material showing staining for transthyretin but not with Congo red was

Table 3 Neuronal cell loss and diameter in sympathetic and sensory ganglia

	Dorsal root ganglia		Sympathetic ganglia	
Case no.	Neuronal cell density, no./mm^2	Diameter of neurons in dorsal root ganglia, μm	Neuronal cell density, no./mm^2	Diameter of neurons in sympathetic ganglia, μm
Early-onset group				
1	4.0 ± 0.9	54.3 ± 8.6	4.2 ± 2.2	24.3 ± 3.8
2	1.9 ± 1.2	53.7 ± 8.8	4.0 ± 1.6	23.7 ± 4.2
3	2.6 ± 1.0	56.0 ± 9.0	1.6 ± 1.4	24.5 ± 3.3
Late-onset group				
12	7.5 ± 1.6	46.2 ± 11.4	46.2 ± 7.4	22.9 ± 4.6
13	4.8 ± 1.2	45.4 ± 9.1	44.8 ± 6.2	19.8 ± 4.6
14	5.8 ± 1.3	49.9 ± 11.4	ND	ND
Controls, n = 4	10.2 ± 3.2	48.3 ± 16.3	60.4 ± 6.6	20.0 ± 4.2

Values of neuronal cell density were expressed as means ± SD for densities on 10 sections as described in Patients and Methods. Values of neuronal cell diameter were expressed as means ± SD for all neurons counted on 10 sections. Control values were obtained from four autopsied cases.

ND = not determined.

abundant in the subperineurial space of the nerve trunk in the late-onset case (see figure 1, E and F), being less plentiful in early-onset cases.

Pathologic findings in visceral organs. In early-onset cases, amyloid deposition was more prominent in the thyroid gland, gastrointestinal tract, pancreas, adrenal gland, and kidney than in late-onset cases (figures 2B and 4). Amyloid deposition in early-onset cases was especially prominent in the thyroid gland and kidney, where deposition was scarce in late-onset cases. On the other hand, in late-onset cases, deposition was greater in the heart and the anterior pituitary lobe than in early-onset cases. Amyloid was scarce or absent in both groups in the posterior lobe of the pituitary gland, liver, and skeletal muscle. The heart weighed 420, 440, and 450 g in early-onset cases, whereas in late-onset patients dying of heart failure, it was 690 and 700 g. In a late-onset patient who died of lung cancer and had relatively short clinical duration of amyloid neuropathy, the heart weight was 380 g. In early-onset cases, cardiac amyloid deposition was prominent in the atrium and the subendocardial region. In the myocardium, amyloid was observed mainly in relation to walls of vessels, particularly arterioles. In the subendocardial layer, myocardial cells showed atrophy, degeneration, and eventual cell loss, producing a histologic picture of amyloid rings (see figure 4A). Among late-onset cases, amyloid was prominent throughout myocardium in two cases (13 and 14), whereas amyloid rings or atrophy of the myocardium was not apparent in any case (see figure 4B). The anterior lobe of the hypophysis showed scarce or no amyloid deposition in early-onset cases, but marked parenchymal deposition was observed in late-onset cases (see figure 4, C and D).

Discussion. In this study, we compared pathologic features of early-onset FAP TTR Met30 cases from endemic foci with those of late-onset cases from non-endemic areas. In anecdotal report of pathologic findings in FAP TTR Met30 patients presenting beyond age 50,[25] the distribution of amyloid deposition differed slightly from findings in the current study. Differences may be attributable to inclusion of late-onset cases from endemic foci in that report; these patients show clinical features similar to early-onset cases in endemic foci.[11] The current study demonstrated that pathologic features of the two groups differed, as has been shown for clinical features.[9-11]

The characteristic finding in early-onset cases was predominant loss of small fibers, including unmyelinated fibers; this agrees with previous reports.[26,27] On the other hand, fiber loss patterns in our late-onset cases were variable; half of the cases showed predominantly small-fiber loss as in early-onset cases, whereas others showed relative preservation of small myelinated fibers. As a whole, the total number of myelinated fibers was more severely reduced in late- than early-onset cases. This difference correlated well with the prominent sensory dissociation noted in early-onset cases in contrast to impairment of all modalities in late-onset cases.[3,9,11] The finding that amyloid deposition and neuronal cell loss were more severe in sympathetic than sensory ganglia in early-onset cases—with the reverse pattern seen in late-onset cases—also correlated with the severity of autonomic symptoms.[3,7-9,11] Furthermore, preferential loss of small neurons in the sensory ganglia in early-onset cases and loss of neurons of all sizes in late-onset cases, as suggested by the mean diameter of remaining neurons, corresponded to clinical differences in sensory involvement. Amyloid deposition and atrophy of myocardial cells in the atrium and subendocardial layer of the myocardium, where the cardiac conduction system is located, explains a more frequent occurrence of cardiac conduction abnormalities and need for pacemaker implantation in early- than late-onset cases.[3,11] On the other hand, diffuse deposition of amyloid with ventricular wall thickening agrees well with frequent observations of cardiac hypertrophy and occur-

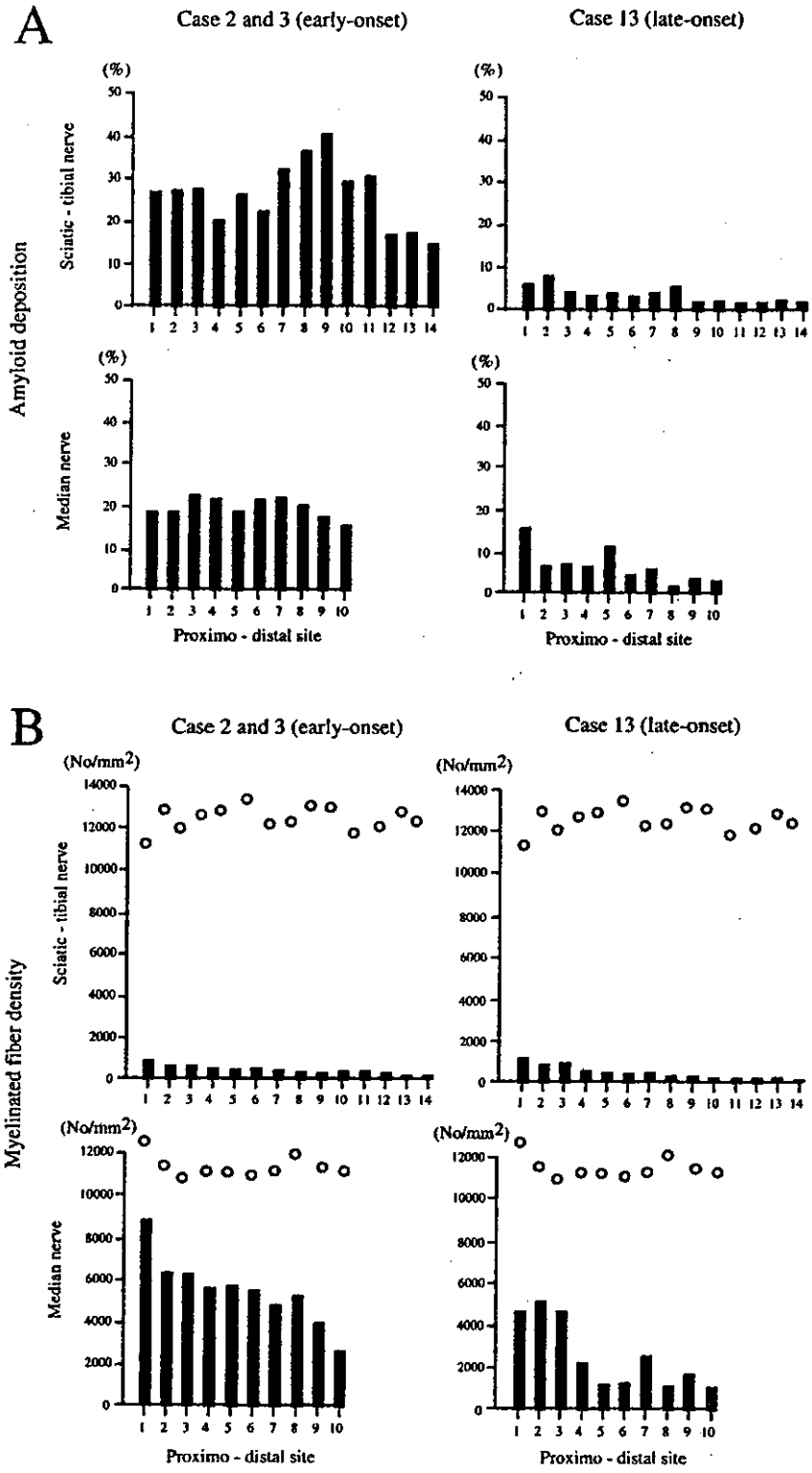

Figure 3. Proportion of amyloid deposition in the endoneurium (A) and density of myelinated fibers (B) in consecutive portions of the sciatic/tibial and median nerves from early-onset cases (Cases 2 and 3) and late-onset case (Case 13). Values for early-onset cases are represented as the means of Cases 2 and 3. Open circles represent normal control values obtained from a subject with nonneurologic disease. In sciatic and tibial nerves, amyloid deposition is more prominent in early-onset cases than in the late-onset case. However, the late-onset case showed considerable myelinated fiber loss despite relative paucity of amyloid deposition. In the median nerve, amyloid deposition also is more severe in early-onset cases than in the late-onset case, whereas myelinated fiber loss is more severe in the late-onset case than in early-onset cases.

rence of heart failure in late-onset cases.[9] Thus, differences in clinical features reported between early- and late-onset FAP TTR Met30 corresponded well to pathologic differences.

A question remains as to why the severity and distribution pattern of amyloid deposition differ between early- and late-onset cases. A longer interval from onset of neuropathic symptoms to autopsy in the early-onset group may explain some of the pathologic differences. The peripheral nervous system, thyroid gland, gastrointestinal tract, pancreas, adrenal gland, and kidney showed more severe amyloid deposition in the early-onset group, consistent with a longer duration of illness. However, the heart and hypophysis showed more prominent deposition in the late-onset group, which had a shorter clinical disease duration. The diffuse amyloid deposition observed in the ventricular myocardium in late-onset cases is

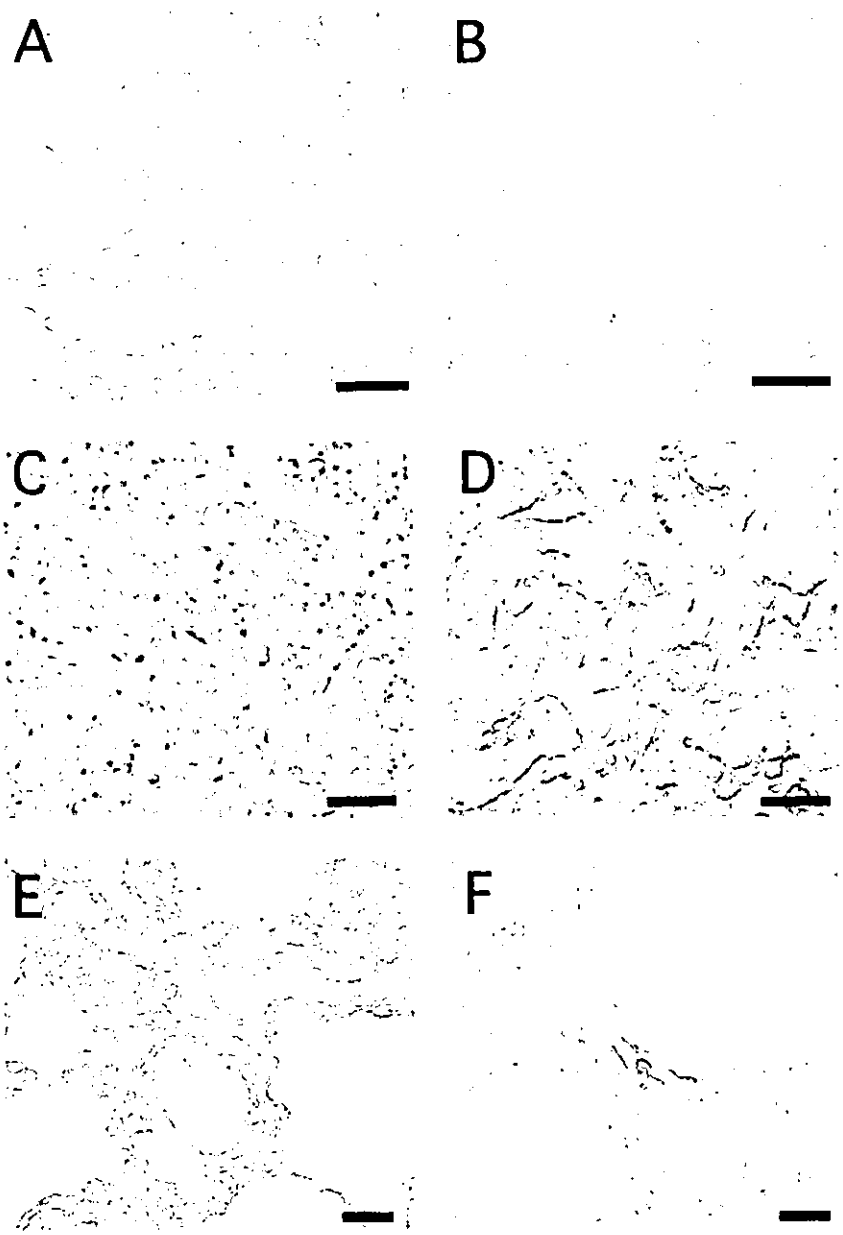

Figure 4. Representative pathologic findings in the visceral organs from early-onset cases (left) and late-onset cases (right). Amyloid deposits are identified by anti-human transthyretin antibody. (A, B) The heart. In the subendocardial layer of an early-onset case (A), myocardial cells show atrophy and amyloid rings are present. In late-onset cases, amyloid is prominent throughout myocardium (B). Amyloid rings or atrophy of the myocardium is not apparent as in (A). (C, D) Anterior lobe of the pituitary gland. Amyloid deposition is scarce in early-onset cases (C), whereas it is conspicuous in late-onset cases (D). (E, F) The thyroid gland. Amyloid deposition was especially prominent in early-onset cases (E), but it was scarce in late-onset cases (F). Bar = 40 μm.

similar to that of senile cardiac amyloidosis with deposition of normal transthyretin protein.[28] Age-related accumulation of amyloid in the interstitium of the anterior lobe of the pituitary gland also has been reported.[29-31] These observations suggest that age-dependent changes in the microenvironment of interstitial tissues in various organs determine the severity and distribution pattern of amyloid deposition in each group. For example, properties of extracellular matrix components including proteoglycans and glycosaminoglycans, which may become components of amyloid,[32] show organ-specific changes with age.[33,34] Interestingly, the posterior lobe of the hypophysis, the liver, and skeletal muscle did not show detectable amyloid deposition in cases with either age at onset. Mechanisms of underlying organ-specific, age-related amyloid deposition still need to be elucidated, but age at onset itself may influence some of the organ-specific amyloid deposition patterns.

Another question remaining is why size dependence of axonal and neuronal cell loss differed between early- and late-onset cases. Even after taking axonal sprouting into account, small myelinated and unmyelinated fibers seemed relatively well preserved in many late-onset cases. Although the pathogenesis of peripheral neuropathy in amyloidosis has not yet been clarified, possibilities might include ischemia from obliteration or dysfunction of small vessels supplying nerves,[35,36] nerve fiber compression or infiltration by amyloid deposits,[26,37] or toxic effects of amyloid precursors.[38-40] Experiments in animals as well as human studies suggest that the nonfibrillar form of transthyretin is present in tissues and exerts cytotoxicity, including oxidative stress,[40] before the congophilic fibrillar form of amyloid can be seen.[38,41]